LONG WAVE BREAKING EFFECTS ON FRINGING REEFS

A Thesis

by

JOHN THOMAS GOERTZ

Submitted to the Office of Graduate Studies of
Texas A&M University
in partial fulfillment of the requirements for the degree of

MASTER OF SCIENCE

Approved by:

Chair of Committee,	James M. Kaihatu
Committee Members,	Kuang-An Chang
	Steven F. DiMarco
	Jane M. Smith
Head of Department,	John Niedzwecki

December 2012

Major Subject: Ocean Engineering

ABSTRACT

Modeling of wave energy transformation and breaking on fringing reefs is inherently difficult due to the unique topography of reefs. Prior methods of determining dissipation are based on empirical data from gently sloping beaches and offer only bulk energy dissipation estimates over the entire spectrum. Methods for deducing a frequency-dependent dissipation have been limited to hypothesized linkages between dissipation and wave shape in the surf zone, and have used bulk dissipation models as a constraint on the overall dissipation for mild sloping beaches. However, there is no clear indication that the constraint on the overall level of dissipation is suitable for the entire reef structure.

Using these constraints the frequency-dependent dissipation rate can be deduced from laboratory data of wave transformation over reefs, taken at the Coastal and Hydraulics Laboratory. The frequency-dependent dissipation rate can then be integrated over the spectrum to derive an empirically-based counterpart to energy flux dissipation. Comparing the bulk energy dissipation estimates for the reef system to the frequency based method allows for the modification of wave breaking parameters in the frequency based estimation. Since this method is based on the Fourier transform of the time series data, it allows the dissipation to be found as a function of the frequency. This analysis shows that there is a correlation between the amount of energy in the low frequencies of the wave spectrum and certain characteristics of the frequency-dependent dissipation coefficient.

DEDICATION

To my loved ones, and all of those that helped me along the way.

ACKNOWLEDGMENTS

This work was conducted under the Surge and Wave Island Modeling Studies under the Coastal Data Field Collection Program of the Coastal and Hydraulics Laboratory, US Army Research and Development Center.

I would also like to thank my advisor Dr. James Kaihatu, for his guidance and direction over the course of this research. I would also like to thank my committee members Dr. Kaung-An Chang, Dr. Steven DiMarco, and Dr. Jane M. Smith for their help, support, and input. I would also like to thank Ernest Smith for collecting the laboratory data used in the analysis present in this thesis.

TABLE OF CONTENTS

Page

Page

LIST OF FIGURES

Page

Page

CHAPTER I

INTRODUCTION

Much of the world's population lives on or near the coast; as a result knowledge of the processes seen in these areas is vital to the infrastructure and the safety of the population. Modeling the wave effects near the shoreline is important because it allows us to estimate what various processes are occurring or could occur. Wave energy throughout the shoaling process is one of the most vital aspects that must be estimated, and is key in finding expected breaking and wave effects in these nearshore environments. However, modeling of the energy transformation and breaking on fringing reefs is especially difficult due to their unique topography. Many coastal areas that are surrounded by nearshore fringing reefs are prone to unique lowland flooding events caused by high waves, wave-induced setup and enhanced low-frequency energy generated by breaking on this topography. As such, research is needed to find better ways to estimate the energy and dissipation in this environment. To this end, this thesis will discuss the current status and history of wave energy calculations in a literature review, followed by a description of applying both new and old methods to an experimental data set. The ultimate goal of this thesis is to provide an improved method of calculating wave energy, in particular to the case of nearshore reef structures, which can be used on any nearshore system.

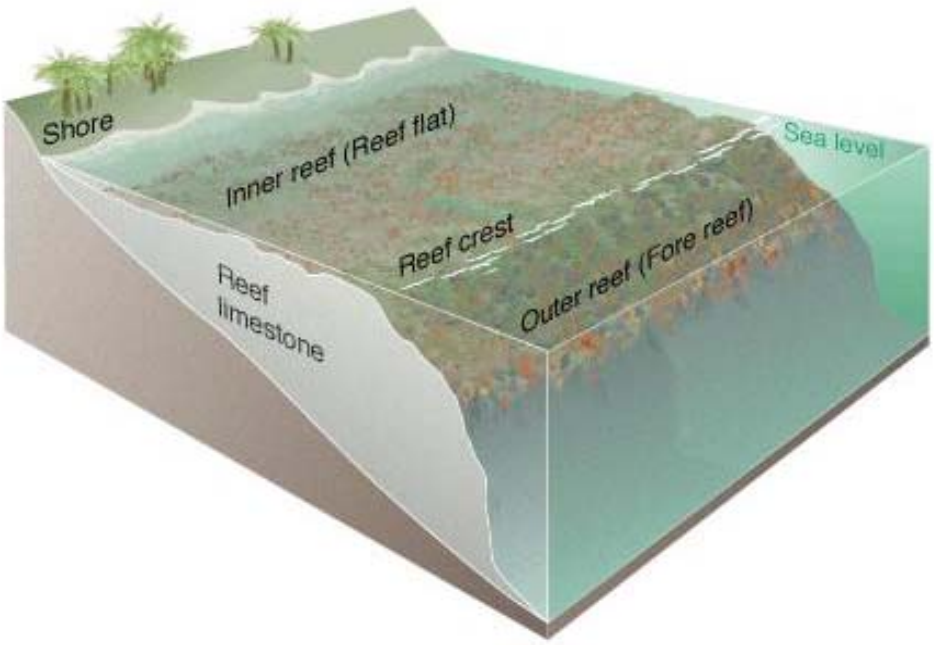

Figure 1: Fringing Reef (From USGS 025-02)

A. Fringing Coral Reef

Coral reefs consist of colonies of tiny animals that grow in tropical marine waters. They are most common in the tropical Pacific Ocean, though some exist in the tropical portion of the Gulf of Mexico and the Indian Ocean (Sverdrup, 2005). Different structure types exist for coral reefs, but one common type is the fringing reef as seen in Figure 1. Many islands in the tropical Pacific are surrounded by fringing reefs, which grow in shallow water close to the coastline. They are characterized by wide-shallow platforms that sharply drop into deep water on the ocean side, while remaining flat from the crest elevation toward the shoreline. Fringing reefs differ from the more typical type of reef, a

platform or barrier reef, which is separated from the mainland by a deep channel or lagoon and can develop hundreds of kilometers offshore. An example profile view of these two types of reefs is shown in Figure 2, and an example of an island that possesses both types of reef can be seen in Figure 3. The red arrow points to the location with the platform reef, where the deep lagoon behind the reef top can be seen. The black arrow points to the location that exhibits a fringing reef, where the reef forms very close to the shore or there is only a small shallow portion of water landward of the reef.

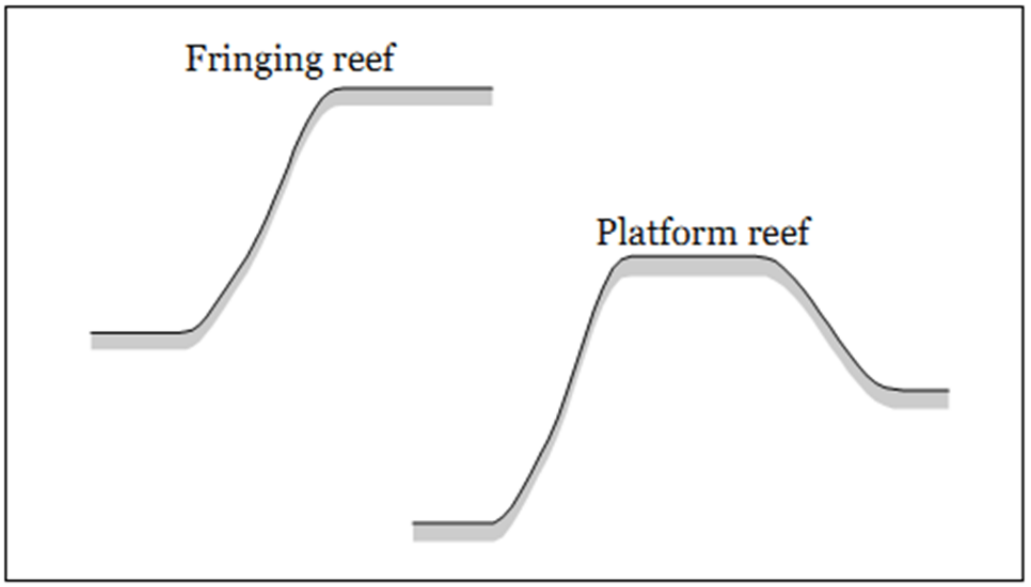

Figure 2: Fringing Reef vs. Platform/Barrier Reef (From ERDC/CHL)

Figure 3: Mana Island, Fiji: Displaying Platform Reef (red) and Fringing Reef (black) (From Google Maps)

The fringing reefs protect coastal areas from wave action by causing waves to break and dissipate their energy offshore of the shoreline. This forced wave breaking can sometimes lead to unique phenomena in the lowland areas near the shoreline. Wave and storm conditions, which would not ordinarily create hazardous conditions, can cause lowland flooding on the shelf of the reef. These conditions are caused by wave-wave interactions amplifying very low frequencies in the area shoreward of the reef crest. Additional damage may also occur during typhoons and hurricanes when the wide, shallow reef shelf causes the surge to build up and allow larger waves to propagate inshore.

Reliable estimates of maximum surges are important to establish flood risk and emergency management protocol. Fringing reefs do not evolve during a storm to mitigate the destructive effects of high waves and surge (as would be the case for a sand beach), allowing these conditions to remain at potentially damaging strength for longer periods of time. Due to wave formation on fringing reefs not following expected responses to storms on sand beaches, further research into the wave energy characteristics is needed. The U.S. Army Corps of Engineers (USACE) began the Surge and Wave Island Modeling Studies (SWIMS) program in 2005 to further this goal. To that end, the program has sponsored this research and spearheaded the development of the data set that will be used in the thesis' analysis.

B. Objectives

This thesis will first show that to estimate the bulk wave energy dissipation of a reef, a combined shallow and steep slope model should be used to obtain a reliable estimate of the dissipation. To obtain more detail about the breaking process over the steep slope, an analysis method is employed whereby estimates of the spectrum of dissipation are made from free surface time series of the data, and the total bulk dissipation is estimated. By comparing bulk energy dissipation estimates from a probabilistic model to this frequency-based method, it is shown that the frequency-based estimates are high relative to the probabilistic methods, and that modification of wave breaking parameters in the frequency estimation can provide better estimates of total dissipation. Since this method is based on the Fourier transform of the time series data, it allows the dissipation to be

found as a function of the frequency, with the only required information from the system being the wave height time series and depth at a given location. The result will be shown to allow for the calculation of both total dissipation and dissipation at specific frequency ranges.

CHAPTER II

LITERATURE REVIEW

Prior methods of determining energy dissipation, such as Thornton and Guza (1983; hereafter TG83), are based on empirical data from gently sloping beaches and offer only bulk energy dissipation estimates over the entire spectrum. There is no clear indication that the overall level of dissipation from TG83 is well predicted for the entire reef structure due to the steep-slope at the toe of the reef. To find a better estimation of the constraints in this steep slope area, Janssen and Battjes (2007; hereafter JB07) can be used to estimate bulk dissipation.

However, it is possible to investigate the breaking process at levels deeper than bulk dissipation estimates. For example, Kaihatu and Kirby (1995) developed a frequency-dependent dissipation mechanism. While the overall dissipation (i.e., integrated over frequencies) is constrained by bulk estimates from probabilistic models, the inter-frequency variation of dissipation allowed this process to influence the nonlinear evolution of irregular waves through the shoaling and surf zones. Theoretical arguments for frequency-dependent dissipation were made by Kirby and Kaihatu (1996; hereafter KK96) and augmented with further data analysis by Kaihatu et al. (2007). Furthermore, KK96 formulated instantaneous dissipation estimates based on the slope of the forward face of the wave, which offered empirical (rather than hypothesized) distributions of dissipation over the frequency range of the spectrum and which were also unconstrained

by a priori bulk estimates. This frequency-dependent dissipation rate can be integrated over the spectrum (Kaihatu and El Safty 2011; hereafter KE11) to derive a bulk dissipation estimate that is comparable to the previously mentioned empirically-based methods, but are instead based on a population of instantaneous dissipation events rather than assumed probability distributions. With suitable adjustment of breaking parameters, the result offers both an energy decay rate over the steep reef face that compares well with established probabilistic models, and a view of the individual breaking waves.

A. Thornton and Guza 1983

One commonly-used method for bulk dissipation calculations for random wave trains is that proposed by Thornton and Guza (1983), an extension of Battjes and Janssen (1978). This was developed by analyzing empirical data from an experiment at Torrey Pines Beach, California, in 1978, which measured wave transformations over gently sloping beaches. These data were shown to support the use of a Rayleigh distribution as a suitable model for the statistics of wave height distribution through the surf zone. In order to describe the wave distributions, a weighted Rayleigh distribution, which limits the upper heights in the breaking zone, is used; this can be seen in Equations 2.1 and 2.2.

$$p_b(H) = W(H)\,p(H) \tag{2.1}$$

$$W(H) = \left(\frac{H_{RMS}}{\gamma h}\right)^n \left[1 - \exp\left(-\left(\frac{H}{\gamma h}\right)^2\right)\right] \le 1 \tag{2.2}$$

The variables in the equation are defined as: H, is wave height; $p_b(H)$, is the breaking wave height distributions; $W(H)$, is the weighted function used to modify the Rayleigh distribution, $p(H)$; H_{RMS}, is the root mean square wave height; γ, is a free parameter which will be discussed later; and h, is the local still-water depth.

The energy dissipation rate of the wave was modeled after that of a periodic wave bore and is represented by Equation 2.3. This rate is a function of: $\overline{f}$, the median frequency of the waves; ρ, the density of the fluid; g, acceleration due to gravity; and B, a free parameter which will be discussed shortly.

$$\varepsilon_b = \frac{\overline{f}}{4}\rho g \frac{(BH)^3}{h} \tag{2.3}$$

The average rate of dissipation (denoted by triangular brackets) is found by summing the dissipation for each broken wave and comes from multiplying the dissipation for a single broken wave by the weighted Rayleigh distribution for breaking waves (Equation 2.4):

$$\langle \varepsilon_b \rangle = \frac{B^3}{4}\rho g \frac{\overline{f}}{4}\int_0^\infty H^3 p_b(H)\, dH \tag{2.4}$$

and after integration, results in the bulk dissipation estimation (Equation 2.5):

$$\langle \varepsilon_b \rangle = \frac{3\sqrt{\pi}}{16}\rho g B^3 \overline{f} \frac{H_{RMS}^5}{\gamma^2 h^3}\left[1 - \frac{1}{\left(1+\left(H_{RMS}/\gamma h\right)^2\right)^{5/2}}\right] \tag{2.5}$$

The B parameter is a breaker coefficient of the wave, and it is based on the proportion of the foam region covering the face of a breaking wave. The γ parameter is an adjustable coefficient that defines the breaker index (ratio of wave height to depth).

Based on these estimations for energy dissipation, TG83 analytically modeled the expected wave height in shallow water for waves approaching normally to the shore as given in Equations 2.6, 2.7, and 2.8.

$$H_{RMS} = a^{1/5} h^{9/10} \left[1 - h^{23/4} \left(\frac{1}{h_0^{23/4}} - \frac{a}{y_d^{5/2}} \right) \right]^{-1/5} \tag{2.6}$$

$$a = \frac{23}{15} \left(\frac{g}{\pi} \right)^{1/2} \frac{\gamma^4 \tan \beta}{B^3 \overline{f}} \tag{2.7}$$

$$y_d = \frac{1}{4\pi} H_d^2 \frac{g^{1/2}}{\overline{f}} \tag{2.8}$$

h_o is the still water depth at a reference location offshore; H_d is the wave height at the offshore reference location; and β is the slope of the bathymetry at the location of interest. Thornton and Guza determined that the resulting truncated Rayleigh distribution gives a good estimate of wave height statistics through comparison to experimental field data. However, they also determined that the model had a general tendency to underestimate dissipation, which they suggest can be fixed via adjustment of the B and γ coefficients.

B. Janssen and Battjes 2007

The model of Thornton and Guza (1983) is useful for general applications. It can be argued, however, that the truncation of the higher wave heights best represents waves traversing a mild-sloping beach. In addition, in contrast to Battjes and Janssen (1978), JB07 allows for the existence of waves higher than the enforced breaking wave height, and thus relaxes both the sharp cutoff and truncation of the Rayleigh distribution performed by Battjes and Janssen (1978). For steep-sloped beaches and areas where the surf zone is fully saturated, the empirically-based weightings for the waveheight distribution discussed by Thornton and Guza (1983) may be insufficient to adequately describe the portion of waves in the distribution higher than the saturation cutoff, since steep slopes may allow waves to shoal beyond their breaking limit.

A model for steep slopes is proposed by Janssen and Battjes (2007), in which they revisit a previous model on steeper beaches by Baldock et al. (1998). The model of Baldock et al. (1998), like that of Thornton and Guza (1983), used the entire Rayleigh distribution for wave heights. However, rather than empirical weightings, Baldock et al. (1998) used the Rayleigh distribution in concert with a single breaking wave height, above which all waves could be considered breaking. This wave height cutoff is not representative of a saturated surf zone (i.e. some fraction of the water depth), but is instead a function of the offshore wave steepness (Battjes and Stive 1985). In this manner, the model is also a weighted distribution, though one that is a step function at $H=H_b$, the breaking wave height.

While the revised model by Baldock et al. (1998) offered good performance with laboratory data, algebraic inconsistencies led to singular behavior at the shoreline. The model by Janssen and Battjes (2007) corrected this behavior. To account for the difference in slope and water level a different Rayleigh distribution is used and integrated with respect to a breaker height H_b, above which the wave is assumed to be breaking. The form of this weighted distribution allows waves to break that are smaller than the reference breaker height. Equation 2.9 shows the new form of the bulk dissipation expression developed by JB07, and after integration results in Equation 2.10. This explicit expression models dissipation on a steep-sloped beach due to the less stringent weighting of the wave distribution function, with $R = H_b/H_{RMS}$.

$$\langle \varepsilon \rangle = \frac{B}{4} \overline{f} \frac{\rho g}{h} \int_{H_b}^{\infty} H^3 p(H) dH \tag{2.9}$$

$$\langle \varepsilon \rangle = \frac{3\sqrt{\pi}}{16} B \overline{f} \rho g \frac{H_{RMS}^3}{h} \left[1 + \frac{4}{3\sqrt{\pi}} \left(R^3 + \frac{3}{2} R \right) \exp\left[-R^2 \right] - erf\left(R \right) \right] \tag{2.10}$$

From the estimate of energy dissipations JB07 are able to further estimate the surf zone wave height evolution as shown in Equation 2.11; where h_x is the beach slope and h_o is a reference offshore depth

$$H_{RMS} = h^{-1/4} \left[\left(h_0^{1/4} H_{RMS,0} \right)^{-1} - \frac{\overline{f} \sqrt{\pi} B}{\sqrt{g} h_x} \left(h^{-3/4} - h_0^{-3/4} \right) \right]^{-1} \tag{2.11}$$

JB07 found that when the algebraic inconsistencies are removed from Baldock et al. (1998) the result is an enhanced dissipation model for steep beaches. The only noted difference between this model and TG83 is the assumed distribution function for the breaking wave heights.

C. Kaihatu and Kirby 1995

Kaihatu and Kirby (1995) derived a nonlinear phase-resolving frequency domain model for dispersive wave shoaling and breaking. They used TG83 as the basis of the model, but modified it to accommodate the phase-resolving paradigm. In addition, incorporation of TG83 into the model required a means to distribute the dissipation across frequencies in the spectrum while constraining the overall dissipation in the spectrum to match the bulk dissipation model. Kaihatu and Kirby (1995) made use of a previously proposed distribution model from Mase and Kirby (1992) and modified the dissipation mechanism (Equations 2.12 through 2.15)

$$\alpha_n = \alpha_{n0} + \left(\frac{f_n}{f_{peak}} \right)^2 \alpha_{n1} \qquad 2.12$$

$$\alpha_{n0} = F\beta(x) \qquad 2.13$$

$$\alpha_{n1} = \left(\beta(x) - \alpha_{n0} \right) \frac{f_{peak}^2 \sum_{n=1}^{N} |A_n|^2}{\sum_{n=1}^{N} f_n^2 |A_n|^2} \qquad 2.14$$

$$\beta(x) = \frac{3\sqrt{\pi}}{4\sqrt{gh}} \frac{B^3 f_{peak} H_{RMS}^5}{\gamma^4 h^5} \qquad 2.15$$

B, γ, and *F* are free parameters that are empirically fit to data; *B* and *γ* have been discussed previously in describing the TG83 breaking mechanism. A_n is the spectrum of complex amplitudes for the free surface time series; f_n is the spectrum of frequencies, corresponding to the complex amplitudes; and f_{peak} is the frequency location of the peak amplitude in the spectrum. The frequency-distributed dissipation mechanism is divided into two parts: α_n, which drains an equal amount of energy across all frequencies, and α_{n1}, which weights the dissipation as a function of frequency squared, biasing the dissipation toward higher frequencies. This latter distribution was shown to be relevant to nearshore breaking wave spectra by Chen et al. (1997). When compared against data, the accuracy of the overall mild-slope equation model shows that this frequency-based dissipation can be used in place of bulk dissipation models.

D. Kirby and Kaihatu 1996

To further clarify the frequency-based dissipation of KK95, Kirby and Kaihatu (1996) used a time-dependent description of instantaneous wave breaking to analyze dissipation characteristics over a random wave train. The instantaneous dissipation based on the eddy viscosity model of Zelt (1991) (transformed to use temporal gradients of free surface elevation) is used to study the breaking characteristics of individual waves. It can be calculated from the transformed version of the eddy viscosity model as shown in Equations 2.16 and 2.17

$$\varepsilon = -\rho\left(\frac{\eta}{h}\right)\left(v_b\eta_t\right)_t \tag{2.16}$$

$$v_b = B^*\gamma^{*2}h\eta_t \tag{2.17}$$

The coefficients B^* and γ^* are not the same free parameters from the bulk dissipation models. For this equation B^*, based on η_t (where the subscript refers to a partial derivative in time) is a value between zero and one, representing whether or not the wave is breaking, and provides a smoothed onset of breaking. The parameter γ^* governs the assumed mixing length. The result can be converted from a dissipation time series to spectral densities of dissipation, as seen in Equation 2.18. In this expression ε_{bn} is the Fourier transform of the instantaneous dissipation, ε, computed directly from measured data

$$S_\varepsilon(n) = \frac{\left\langle\left|\varepsilon_{bn}\right|^2\right\rangle}{2\Delta f} \tag{2.18}$$

Using the smoothed spectral density of the dissipation along with the spectral density of the complex amplitudes (A_n) from Equation 2.19, KK96 then calculated an estimate of the dissipation rate, α_n, from Equation 2.20

$$S_\eta(n) = \frac{\left\langle\left|A_n\right|^2\right\rangle}{2\Delta f} \tag{2.19}$$

$$\alpha_n = \frac{1}{2C_{gn}\sqrt{2\Delta f}}\frac{1}{\rho g}\frac{\sqrt{S_\varepsilon(f_n)}}{S_\eta(f_n)} \tag{2.20}$$

Using this process, they showed that the time series itself could be used to directly estimate the dissipation rate without prior constraint by probability distributions based on bulk dissipation models.

E. Kaihatu and El Safty 2011

Bulk energy dissipation is generally quantified as a change in energy flux, such as in TG83 and JB07. However, these parametric formulations differ based on the exact weighting function used. A more detailed and robust model for estimating this bulk dissipation offers more insight into the nature of the energy dissipation. One example of this was developed by Kaihatu and El Safty (2011), based on work by KK96 and Kaihatu et al. (2007). Using these prior results, KE11 devised a way to calculate the bulk dissipation based on a summation over frequency of detailed dissipation estimations and instantaneous breaking, Equation 2.21

$$-D = -\rho g \sum_{n=1}^{N} C_{gn} \left|A_n\right|^2 \alpha_n \qquad 2.21$$

D is the total dissipation; and C_g is the group velocity of the wave. By summing over the full series spectrum of frequencies they arrived at a good estimate of bulk dissipation, circumventing an overdependence on probabilistic distributions and free parameters. In addition, summing over portions of the frequency spectrum can also be used to calculate the dissipation in specific frequency ranges.

F. Experimental Data Set

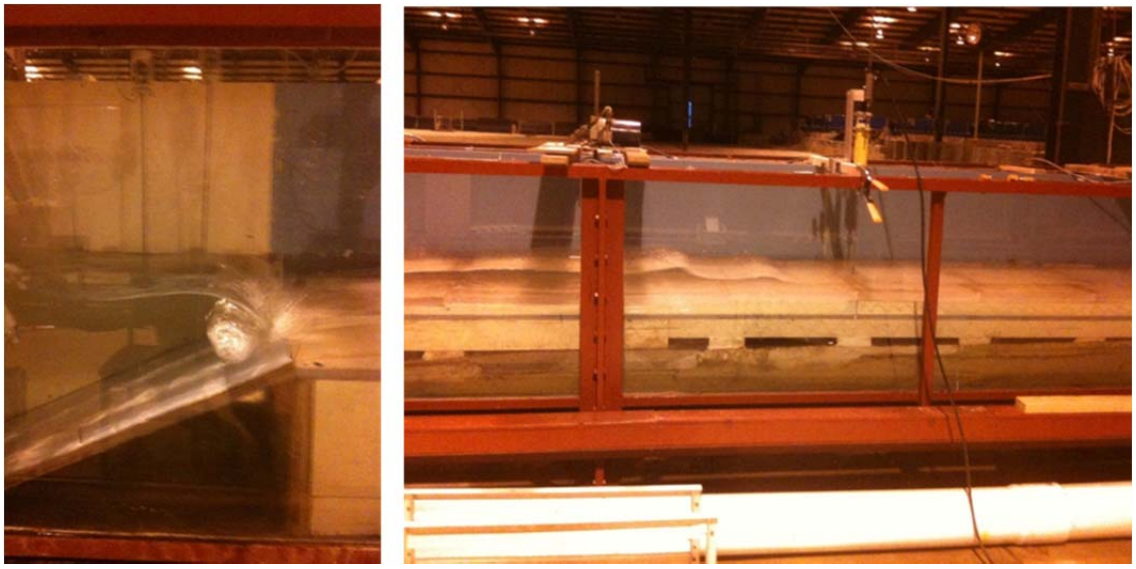

Figure 4: US Army Corp of Engineers Experiment

Data are required to discern the empirically-based dissipation function. The data set used for the dissipation analysis comes from an experiment performed by the SWIMS program at the Engineer Research and Development Center, Coastal and Hydraulics Laboratory, in the fall of 2010. The data set is comprised of random waves over a prototype fringing reef in a 2D wave flume. The flume is a 3-ft wide and contained a 1:50 model to prototype scale reef. The modeled reef consists of either a 1:2.5 or a 1:5 reef front slope and a 24-ft long reef section at a slope of 1:100 that is constructed of molded acrylic to represent a reef bathymetry. Photos of the wave flume while an experimental study was in progress can be seen in Figure 4. The goal of the experiment was to collect wave and run-up data over a range of wave heights and periods, water

levels, and reef roughness. Forty-three design wave conditions were run for each reef front slope and can be seen in Appendix A. Twelve gages were placed along the flume, as seen in Figure 5, to measure free surface elevations versus time with a sampling rate of 20 Hz.

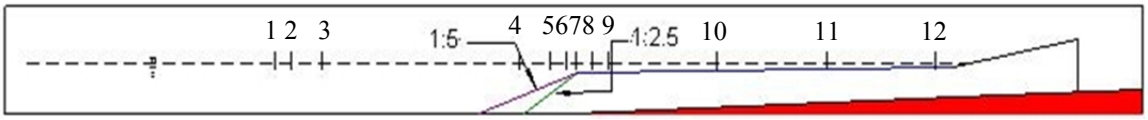

Figure 5: Wave Flume Diagram with Gage Locations (vertical lines)

This data set is chosen for this study for several reasons. First and foremost is the fact the experiment models the wave effects for a fringing reef. The acrylic reef top is modeled after data scans of an actual fringing reef located in Guam. This experiment also attempts to recreate the natural roughness of a reef by including a rough top for the acrylic reef. This experiment also contains a dense gage concentration at the top of the steep slope, where the wave energy exhibits the highest degree of spatial variation. Other similar experiments use a sparser gage distribution near the reef crest, and thus do not capture the rapid evolution of wave energy (heights) near the crest.

CHAPTER III

PROBABILISTIC MODEL

A. Free Parameters

Both probabilistic models (TG83 and JB07) contain free parameters. The TG83 model contains two parameters, B and γ, and the JB07 model contains just the B parameter. These parameters relate to several different properties of the wave breaking system. While both of these parameters have a basis on physical characteristics, they act as tunable parameters (calibration parameters) for the system.

Due to the tendency of the TG83 model to underestimate dissipation, tuning of these parameters is required for an optimal representation of the data. In order to tune these parameters to the system, the root-mean-square wave height (H_{RMS}) estimation of TG83 will be used. The directly calculated H_{RMS} for the system is found by taking the time series data and using the zero-upcrossing method. Using the directly calculated wave height as a metric, a comparison to the estimated H_{RMS} from TG83 allows tuning of the B and γ parameters. This results in a set of tuned parameters that are a best fit to this lab data set for use in wave height and dissipation estimation. Since the JB07 model estimate for wave height and dissipation only contains the B parameter, the value found from tuning TG83 will be used.

B. H_{RMS} Estimation

During the tuning of the TG83 parameters a trend in the H_{RMS} estimation was observed. Despite the tuning of the parameters to get a best fit comparison, the values that were found at the slope of the reef were still underestimating by a factor of 15 - 30%. An example of this can be seen in Figure 6; the values from the tuned H_{RMS} estimations for the shelf of the reef show a close estimate for the wave height while the model estimate at the slope underestimates the height.

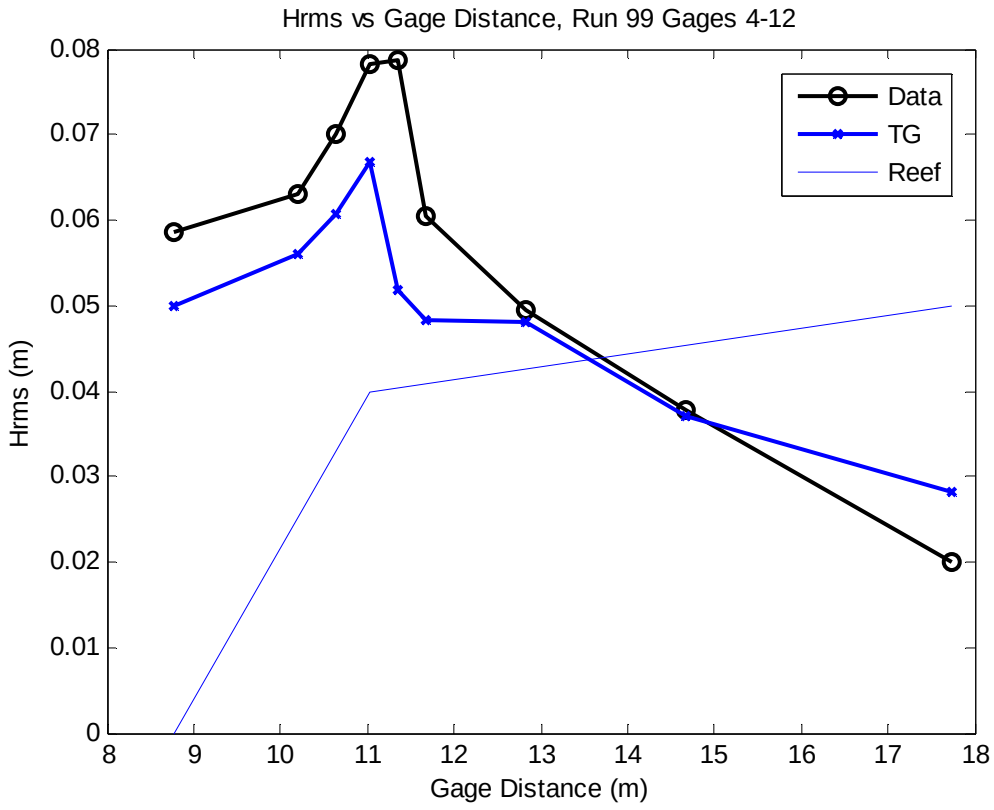

Figure 6: H_{RMS} of TG83 vs. Directly Calculated H_{RMS}

From this we can see that, despite tuning of the parameters, TG83 does not give an effective estimation over the steep slope portion of the reef. As previously stated, this can be expected, as it was developed for applications over mild-sloping beaches. Since TG83 gives poor estimates over the entirety of the reef, JB07 was considered to seek a better estimate. The JB07 model also contains an estimate for H_{RMS} that is used to compare to the directly calculated values. The result of this can be seen in Figure 7 (same experimental case as Figure 6). As expected the JB07 model gives a much better approximation at the steep slope of the reef, but on the shelf where the very mild slope exists, the model fails to give realistic values.

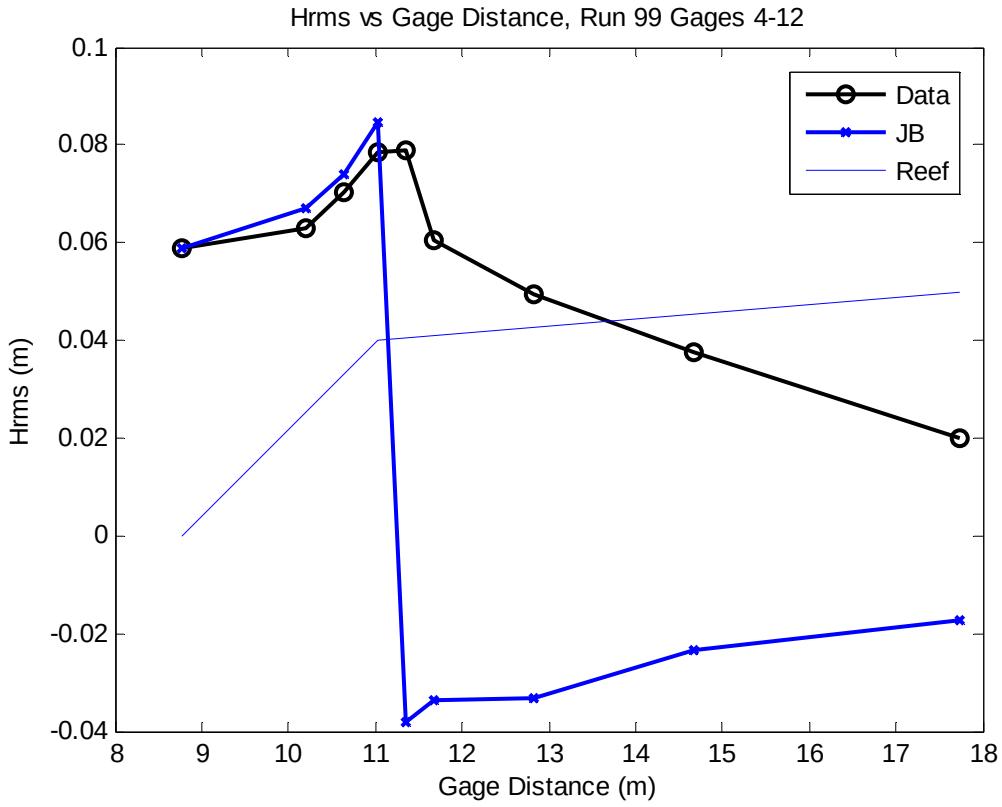

Figure 7: H_{RMS} of JB07 vs. Directly Calculated H_{RMS}

The negative values for the model on the reef shelf can be attributed to the slope value in the model equation. This value is in the denominator of a negative term, and when the slope is very small, as is the case on the reef shelf, results in a large negative number. More plots of H_{RMS} comparisons showing these relations of model to data for TG83 and JB07 can be seen in Appendix B.

C. Model Combination

Neither model is effective at estimating the wave height over the entire reef system. It is clear that this will hold true for the bulk dissipation estimation as well. In order to derive a total bulk dissipation estimate over the whole reef system a combination of the two models is used. Since the JB07 model provides the best estimate for wave height at the steep slope portion it will be used for the gages in that location.

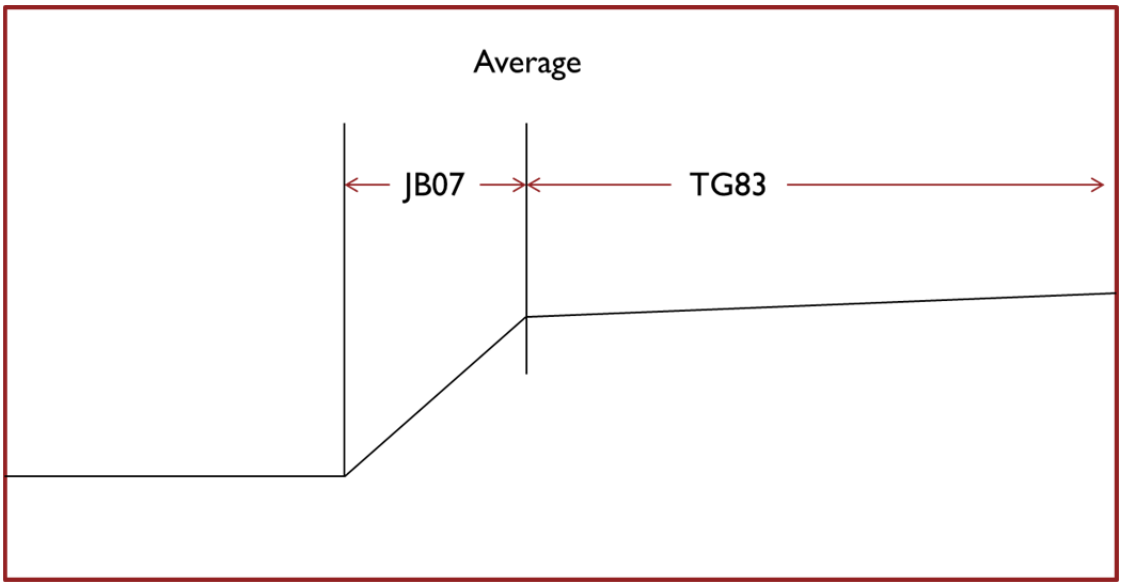

Figure 8: Dissipation Zones for Combined Probabilistic Model

TG83 will be used for the estimation of the last four gages on the shelf of the reef. Gage number seven is located at the transition between the steep slope and mild slope. At this location a weighted average for H_{RMS} and a normal average for dissipation estimates will be used. Figure 8 shows the location of the regions in which each model will be used.

The resulting H_{RMS} estimation from the combined models can be seen in Figure 9. Combining the models results in one continuous solution for wave height estimates, and can be applied to the dissipation estimates of the models. More plots of the combined models for H_{RMS} can be seen in Appendix B.

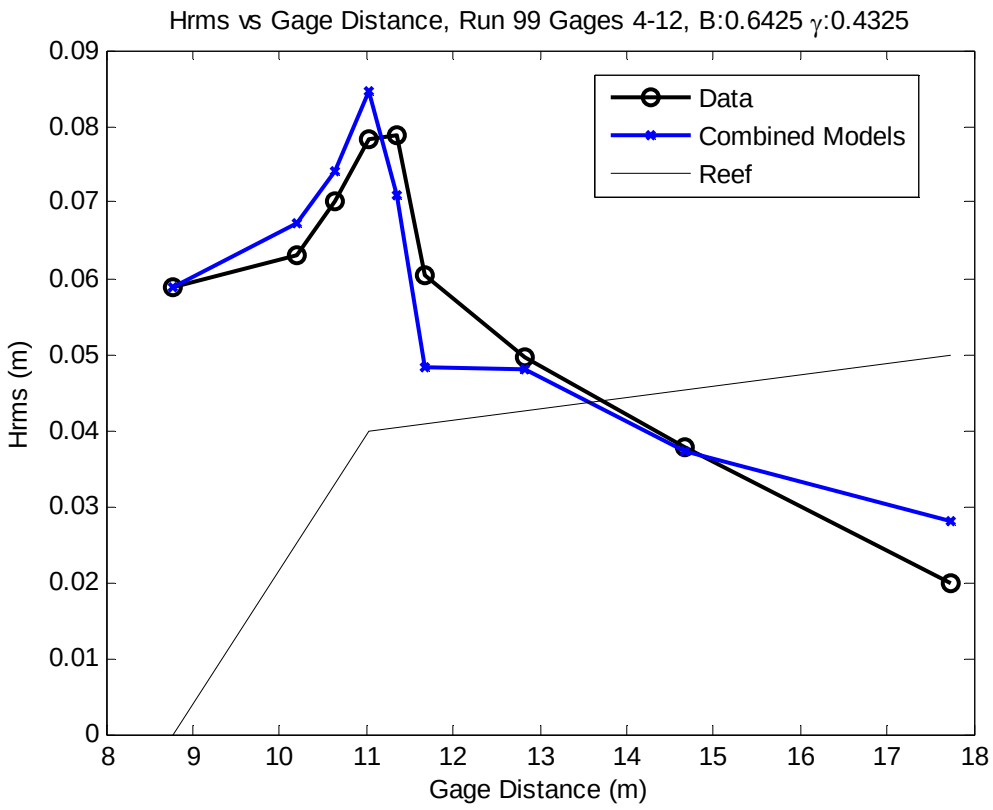

Figure 9: Combined Model H_{RMS} vs. Directly Calculated H_{RMS}

D. Dissipation Analysis

The result of combining the two models is one model that can estimate both H_{RMS} and bulk dissipation for this system. The largest downside to this model is the limitation of only being capable to calculate the bulk dissipation. This limits on the wave characteristic analysis that can be performed. The results of the bulk dissipation can be seen in Figure 10.

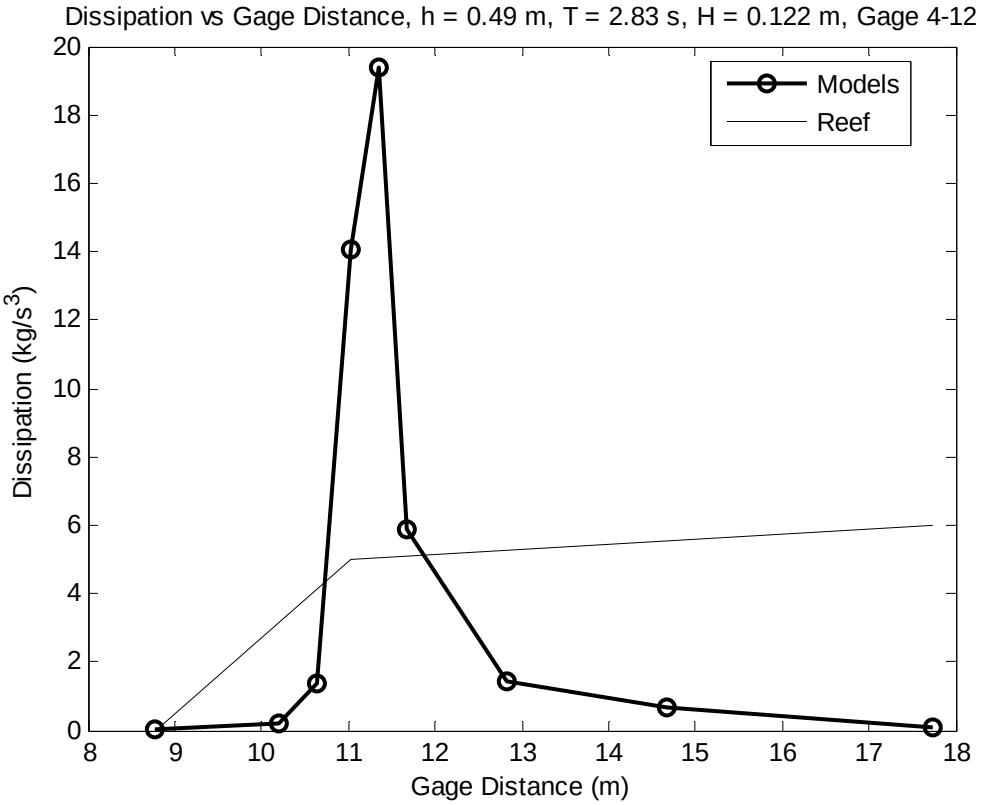

Figure 10: Bulk Dissipation for Combined Probabilistic Models

As expected, there is little to no dissipation in the system as it approaches the reef slope. There is then a sharp increase to peak dissipation at the top of the slope, where the waves are being forced to break by the sudden change in water depth. On the long flat portion of the shelf the dissipation continues, however at a much lower rate.

While the bulk estimation of dissipation is in itself valuable, the goal of this research is in the analysis of the wave energy of the system at a finer level. These results do not allow analysis at these levels due to the inability of this model to discern more than the bulk dissipation. However, as will be discussed, this estimation can be used as a metric to further tune analysis methods that can analyze energy dissipation at non bulk levels.

CHAPTER IV

FREQUENCY-BASED DISSIPATION

A. Dissipation Rate Calculation

As discussed previously, the method of KK96 is used to calculate the dissipation rate, α, using Equation 2.20. This rate is a representation of a distribution of instantaneous dissipation rates over the frequency range of the spectrum whose overall sum over the spectrum is constrained by a probabilistic distribution. It is calculated from a combination of the smoothed spectrum of the free surface time series and the instantaneous dissipation time series based on the Zelt (1991) eddy viscosity formulation. The calculation of these spectra is accomplished using the Fast Fourier Transform of Matlab. The smoothing to the spectrum is performed using Bartlett averaging: the data set is broken up into a set of twenty-three realizations each consisting of 1024 individual points, and then these sets are averaged together. With a sampling time step of 0.05 seconds the resulting Nyquist frequency for the data set is 10 Hz and the fundamental frequency is 0.0195 Hz. Due to the sensitivity of free surface elevation time series data in the high frequency to noise, the data set will be analyzed to one half the Nyquist frequency, or 5 Hz.

An example plot of the smoothed spectrum of instantaneous dissipation events can be seen in Figure 11. The three gages chosen as key points of interest in the system are gages six, eight, and ten. Gage six is located half way up the reef slope and represents a

location where the waves are just starting to shoal and break due to the change in water depth. Gage eight is located just past the toe of the slope where most of the waves are breaking. Gage ten is located far up the shelf of the reef after much of the wave energy has already been dissipated. Due to the nature of random waves, the instantaneous dissipation is a "spike" time series, which consists of a set of discontinuous impulses. The resultant spectra of this type of time series is "white", exhibiting constant energy levels across all frequencies. The result is a spectrum that does not change with frequency.

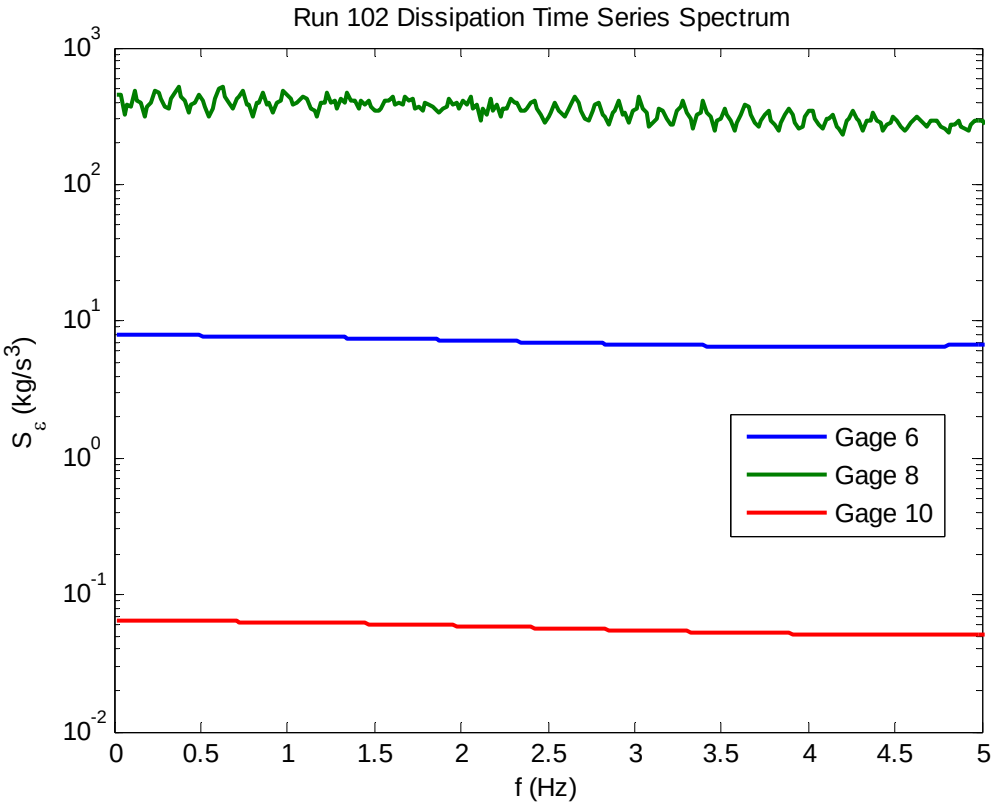

Figure 11: Smoothed Time Series Spectrum of Instantaneous Dissipation

The magnitude of each plot can be related to the amount of instantaneous dissipation occurring at each gage in relation to the other gages. As expected, the amount occurring at gage ten is the least since most of the waves have already broken, and the most frequent occurrence of instantaneous dissipation is at gage eight where most of the waves are breaking.

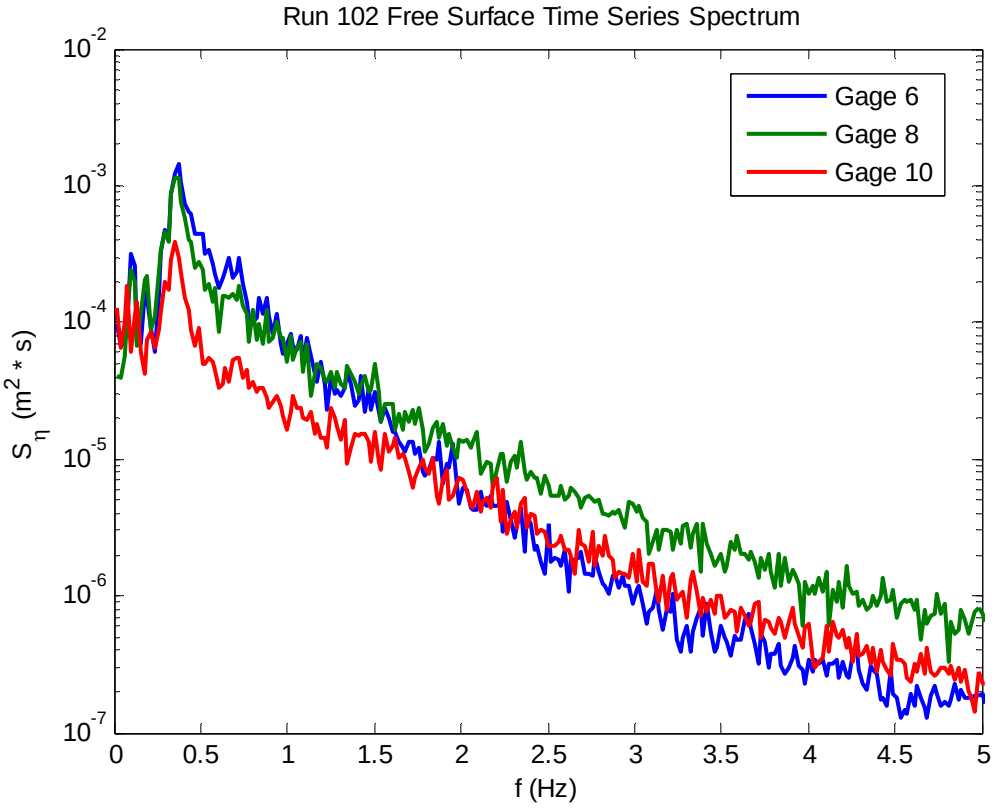

Figure 12: Time Series Spectrum at Key Gages

The result of the spectrum of instantaneous dissipation being constant with frequency is the dissipation rate depends on and is proportional to the inverse of the time series spectrum. This relationship, first seen comparing Equation 2.20, can also be seen

comparing Figure 12 and Figure 13. This further implies that there is a dependence of the dissipation rate on frequency in the system.

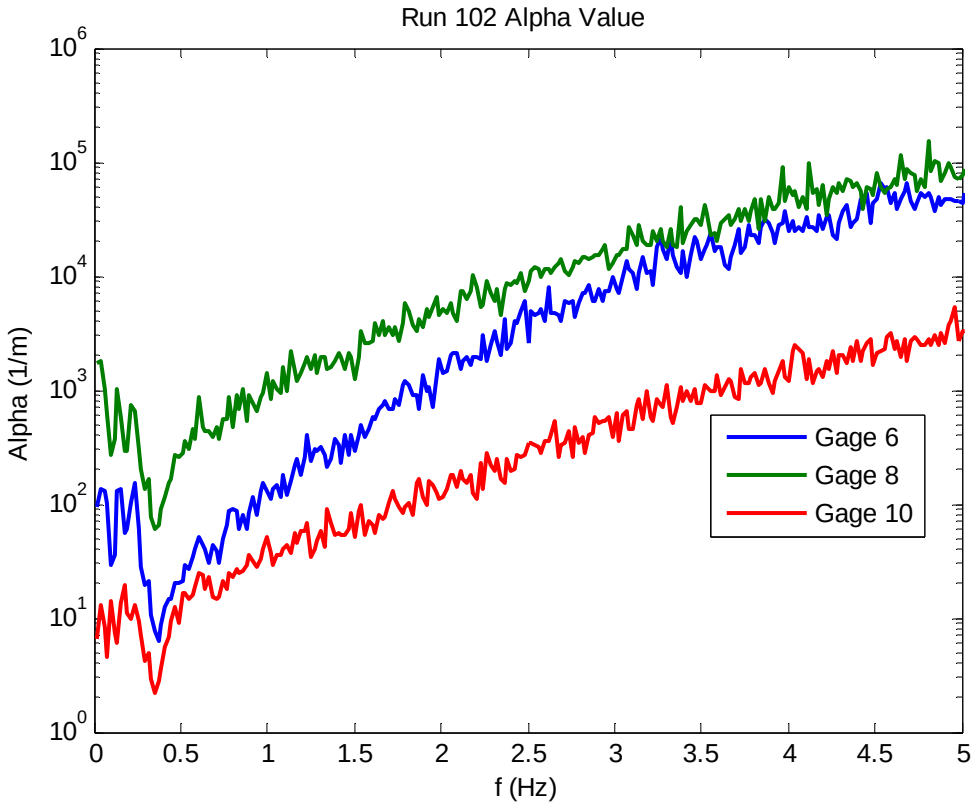

Figure 13: Alpha, Dissipation Rate for Key Gages

B. Bulk Dissipation Estimate

The bulk dissipation of the system can be estimated from the frequency-based dissipation rate α_n using Equation 2.21 proposed by KE11. This is found by summing the individual dissipation rates, along with the complex amplitudes and group velocity, across all frequencies. This bulk dissipation is similar to that of the combined

probabilistic models, though it is derived via frequency-based analysis of the data. The result of this estimate for bulk dissipation at each gage location can be seen in Figure 14. More plot comparisons between the unadjusted frequency based analysis method and modeled values can be seen in Appendix C.

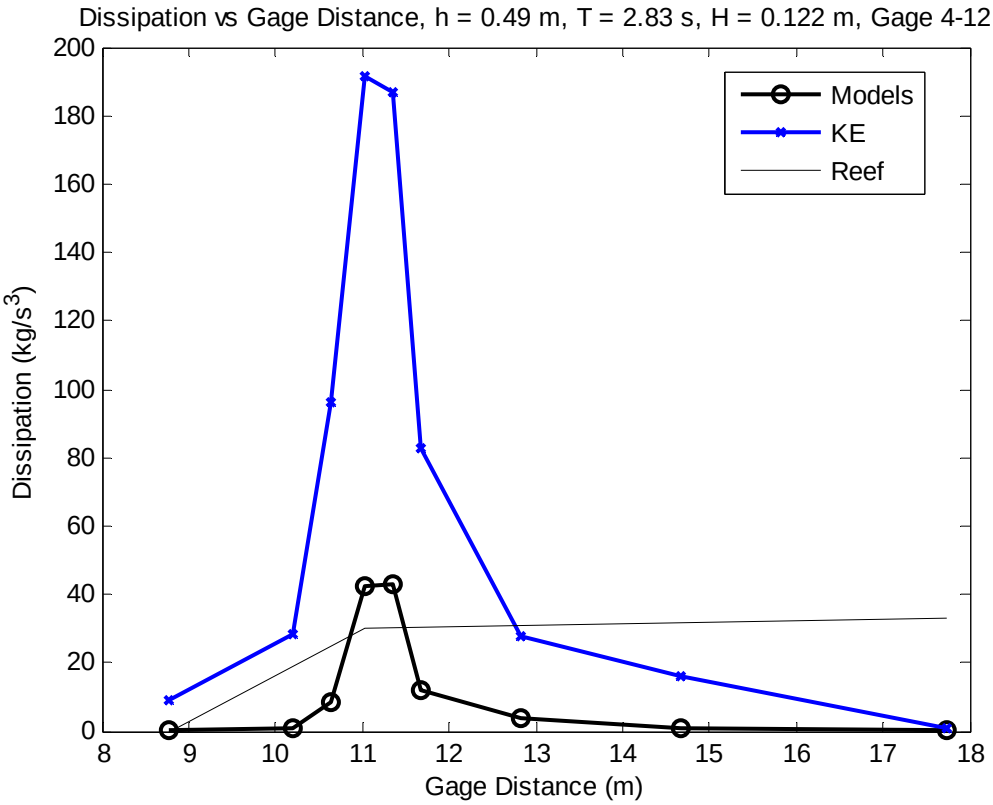

Figure 14: Frequency and Probabilistic Based Dissipation vs. Gage Distance

From this we see that the frequency-based analysis overestimates the amount of dissipation at each gage location relative to those from the probabilistic models, the parameters for which were tuned to the wave height data. This is likely due to the fact that, as previously stated, the instantaneous dissipation is a function of the inverse of the

free surface time series spectrum. Since this spectrum tends to get very small at high frequencies, α can get very large. Another process affecting these large values for alpha can be the sensitivity of the high frequencies to noise, which as stated before is the reason the value is only calculated to half the Nyquist frequency. A final possible reason for this discrepancy is due to the inherent assumption in Zelt (1991) that a breaking solitary wave over a flat bottom is a suitable proxy for breaking waves in general scenarios. This latter assumption is the basis for further adjustments to the frequency-based analysis.

C. Zelt 1991 Constraint

Due to overestimation of the frequency-based bulk dissipation, further analysis into the breaking mechanisms of instantaneous dissipation rate was needed. The instantaneous dissipation events, ε, used in the calculation of α_n come from the eddy viscosity model (Equation 2.16), which is in turn based on a parameter B^*. This parameter, which ranges between zero and one, provides a smoothed onset of breaking dissipation values when the breaking criterion is exceeded. The criteria that predict breaking and determine the value of B^* can be seen in Equation 4.1 and Equation 4.2

$$B^* = \begin{cases} 1 & : \eta_t \geq 2\eta_t^* \\ \eta_t / \eta_t^* - 1 & : \eta_t^* < \eta_t < 2\eta_t^* \\ 0 & : \eta_t \leq \eta_t^* \end{cases} \tag{4.1}$$

$$\eta_t^* = k\sqrt{gh} \tag{4.2}$$

When the temporal gradient of free surface elevation is below the critical value shown in Equation 4.2, the wave is not actively breaking and B^* is correspondingly zero. When this gradient is greater than twice the critical value, $B^* = 1$, and the wave is fully broken. There is a transition between these two values which represents waves in the process of breaking. Of note is the empirical nature of Equation 4.2. The normal value of k in Equation 4.2, which is 0.3, was derived by Zelt based on a ratio of breaking wave height to depth in order to replicate the breaking of a solitary wave, as mentioned previously.

D. Modified Dissipation

Use of this solitary wave estimate causes an overestimation of the dissipation (relative to probabilistic models) because a wave group will break differently and with different characteristics from that of a single wave. A modification must therefore be found. By tuning the value of k in Equation 4.2 to a larger value there, it will limit the number of waves breaking at each gage location. This tuning will reduce the amount of energy being lost in the high frequencies, and will reduce the estimate on total dissipation in the system.

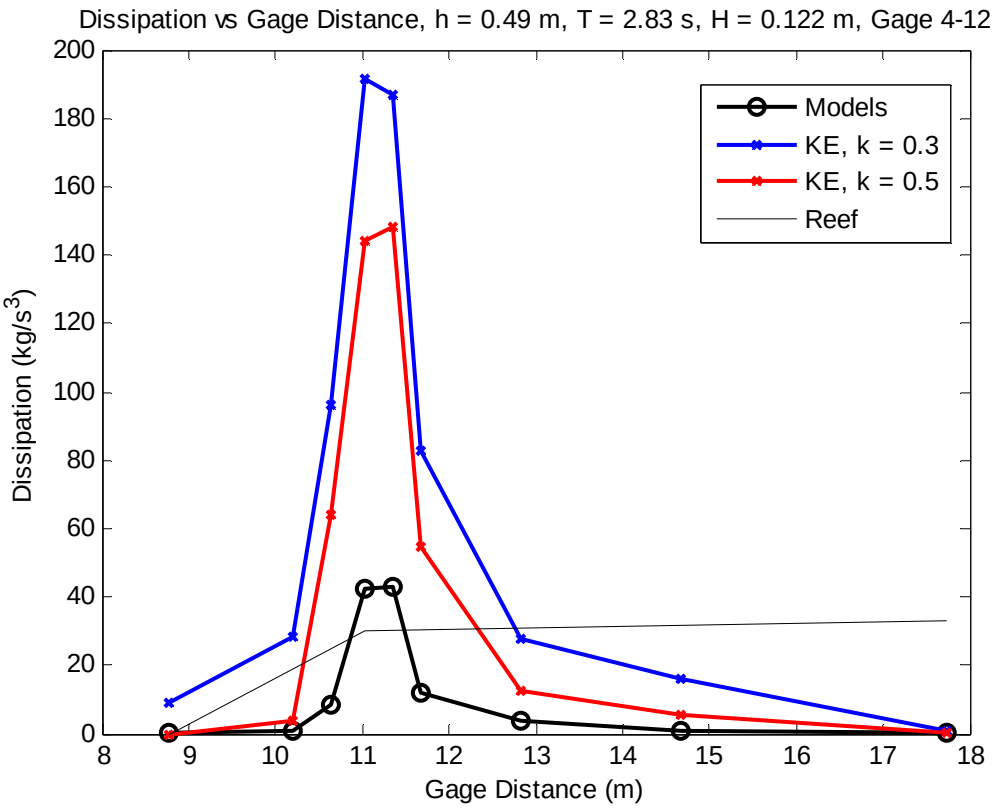

Figure 15: Frequency and Probabilistic Based Dissipation vs. Gage Distance, k = 0.5

The result of changing this value can be seen by comparing Figure 15, Figure 16, and Figure 17. Changing k to 0.5, as seen in Figure 15, does not have much of an effect on the overall dissipation, though it does show a lowering of total dissipation at each gage. Changing k to 0.7, as seen in Figure 16, tunes down the dissipation at the gages four, five, ten, eleven, and twelve to an amount more in line with that of the probabilistic models. At this tuning the amount of dissipation at the top of the reef slope is still over estimated.

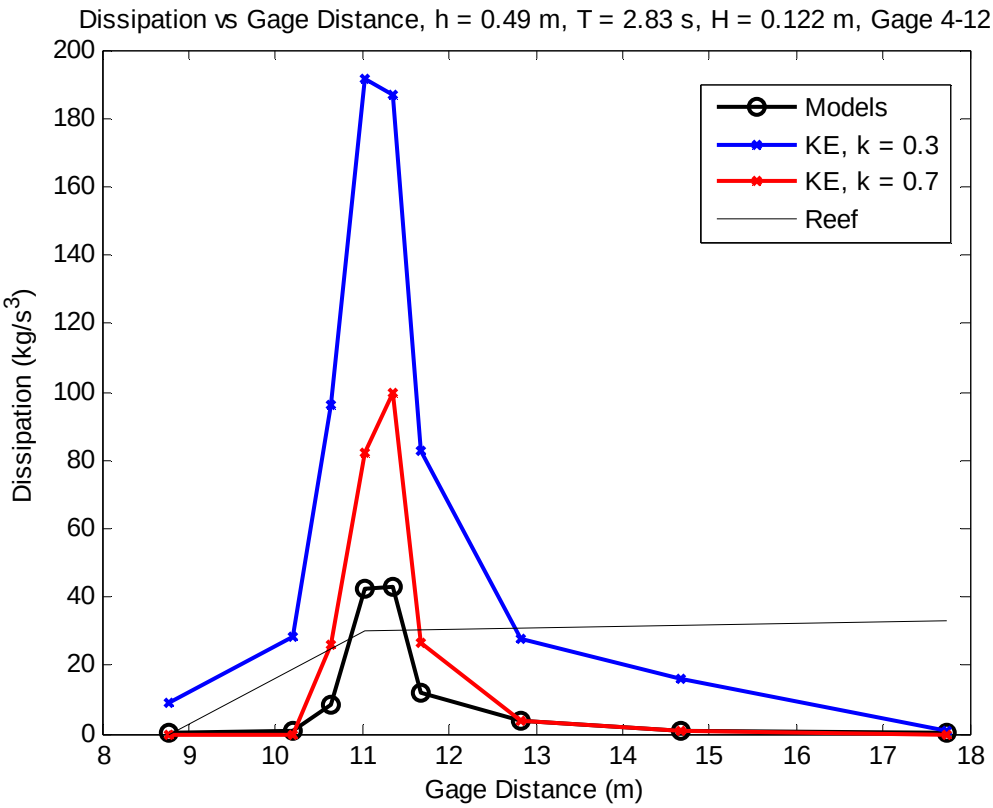

Figure 16: Frequency and Probabilistic Based Dissipation vs. Gage Distance, k = 0.7

Figure 17 shows the result of changing the breaking value k to 0.9. At this level of tuning for the analysis the amount of dissipation at the most energetic wave breaking locations, at the top of the steep reef slope, are in line with that of the probabilistic models. With this amount of tuning though, the dissipation estimate at the gages on the mild slope of the reef are underestimated. More plots of tuning effects on the frequency based dissipation compared to modeled values can be seen in Appendix C.

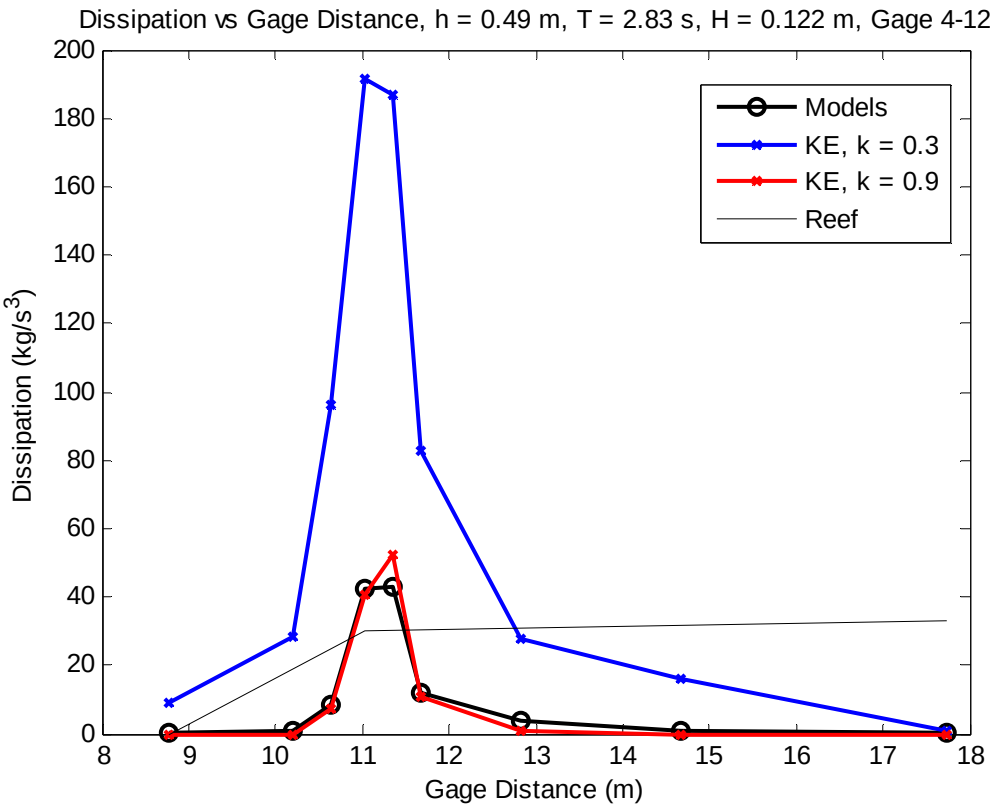

Figure 17: Frequency and Probabilistic Based Dissipation vs. Gage Distance, k = 0.9

Multiple values for the breaking limiter for the reef might be expected, as it is not only a function of the wave energy, but also the depth and slope of the bathymetry at each location. To account for this, the breaking index of 0.9 will be used for k at gages six through nine, where the wave set is the most energetic, and there is the largest change in water depth. The lower breaking index of k = 0.7 will be used for gages four, five, and ten through twelve, where the wave set is less energetic and the bottom slope is mildest. These areas coincide with locations where the bathymetry will have less of an effect on shoaling and breaking of waves, such as an area where the bathymetry has just changed, or an area of small slope, which has less effect on shoaling. These modifications result in

an estimation of bulk dissipation based in the frequency domain that closely approximates that of the combined probabilistic models, as seen in Figure 18.

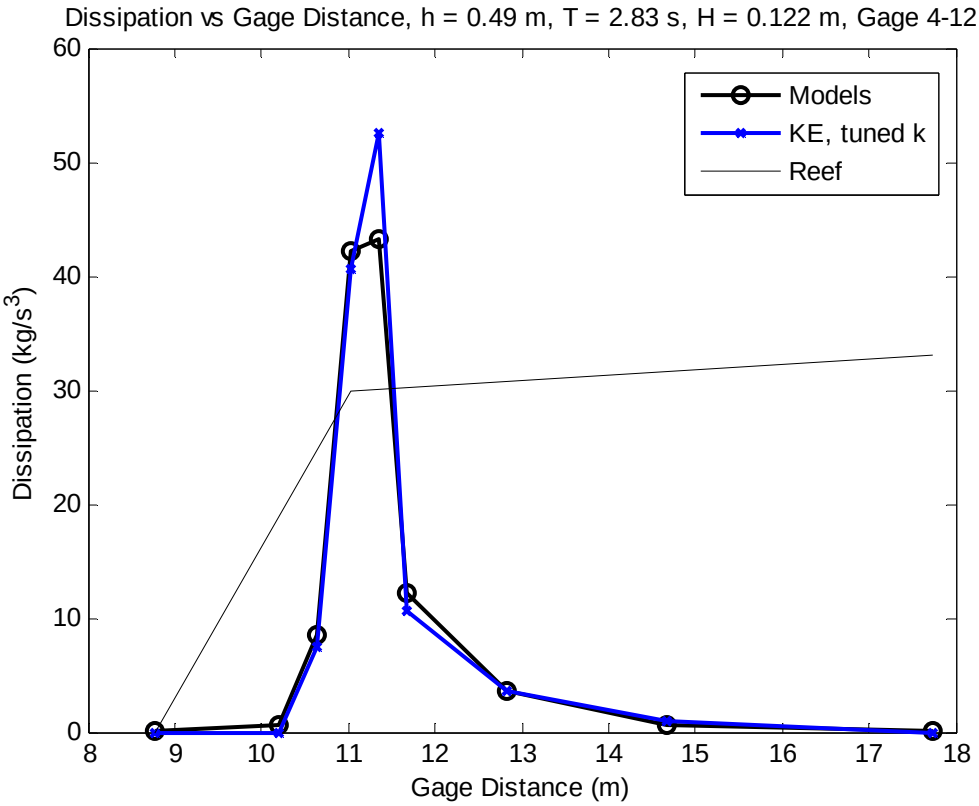

Figure 18: Frequency and Probabilistic Based Dissipation vs. Gage Distance, Changing Breaking Modification

CHAPTER V

FREQUENCY-BASED ANALYSIS

The tuning of the eddy viscosity breaking parameter results in an analysis method that is based only on the time series of the free surface elevation and the depth at the region. This method allows for the estimation of dissipation with no further reliance on probability distributions and corresponding weightings. It allows for analysis of wave energy effects for not only bulk dissipation but also in finer detail than the pure bulk probabilistic models would allow. To this end we analyze, using the same data set from the SWIMS-2D flume experiment, the differences seen in dissipation based on varying incident wave conditions over the model reef system. We also compare bulk dissipation estimates to those of dissipation of events occurring in the low-frequency band of the spectrum.

A. Varying Incident Wave Height

Variations in the incident wave height included in the experiment can be expected to result in different breaking wave conditions. Larger wave heights will give more total energy for the whole system while smaller waves will have less total energy in the entire system. This can be observed in Figure 19, which shows gages four through twelve of the system. Gages one through three are not shown, as they are in the flat pre-reef portion of the wave flume where no breaking is occurring. What is important to note is the amount of dissipation occurring at each gage along with the location of the peak dissipation. We can see from this that as the incident wave height is increased the

amount of dissipation in gages four, five and six, which are located on the steep slope, increases at a larger rate than at the gages on the reef shelf. Of note is that the amount of dissipation at gage six increases at a larger rate than at gage seven. This implies that the increase in wave height and total energy in the system is not felt as much on the reef shelf, but is felt mostly on the steep slope portion of the reef.

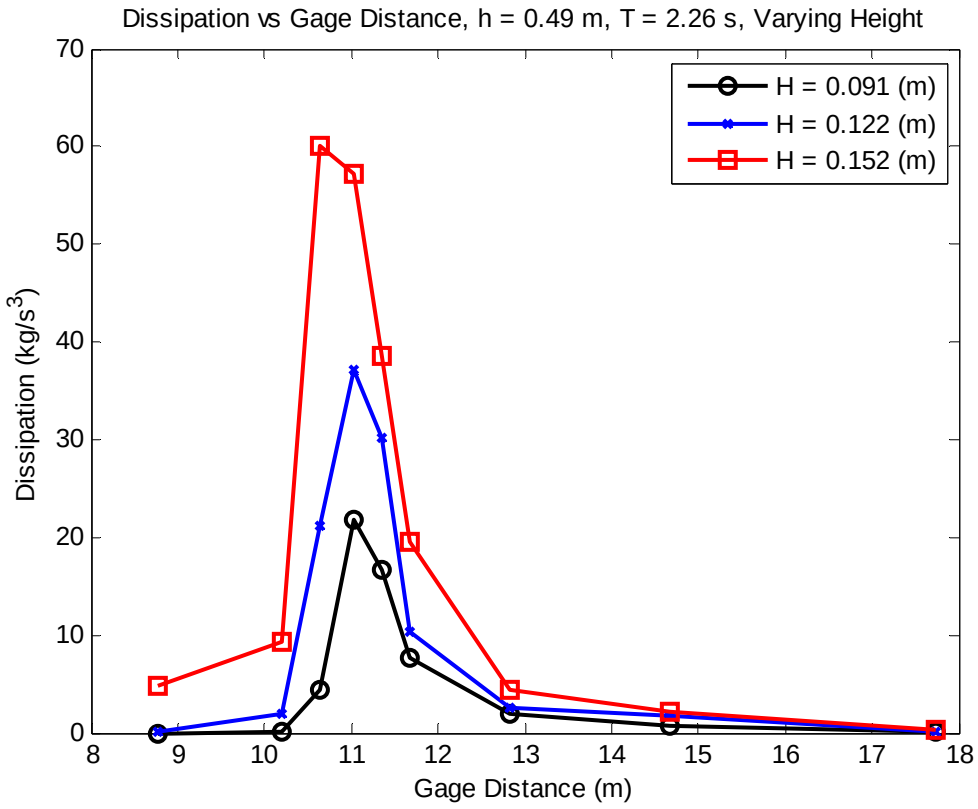

Figure 19: Total Dissipation vs. Gage Distance, Varying Incident Wave Height

While this analysis could also have been performed using the probabilistic models, the frequency-based method allows us to examine dissipation in specific frequency bands, such as the low-frequency waves. This can be seen in Figure 20 where we analyze only

the low-frequency waves (those in the range from zero to one half of the peak frequency). We can see from this figure that waves in the lower frequencies follow the same trend that we see in the full bulk dissipation of the system.

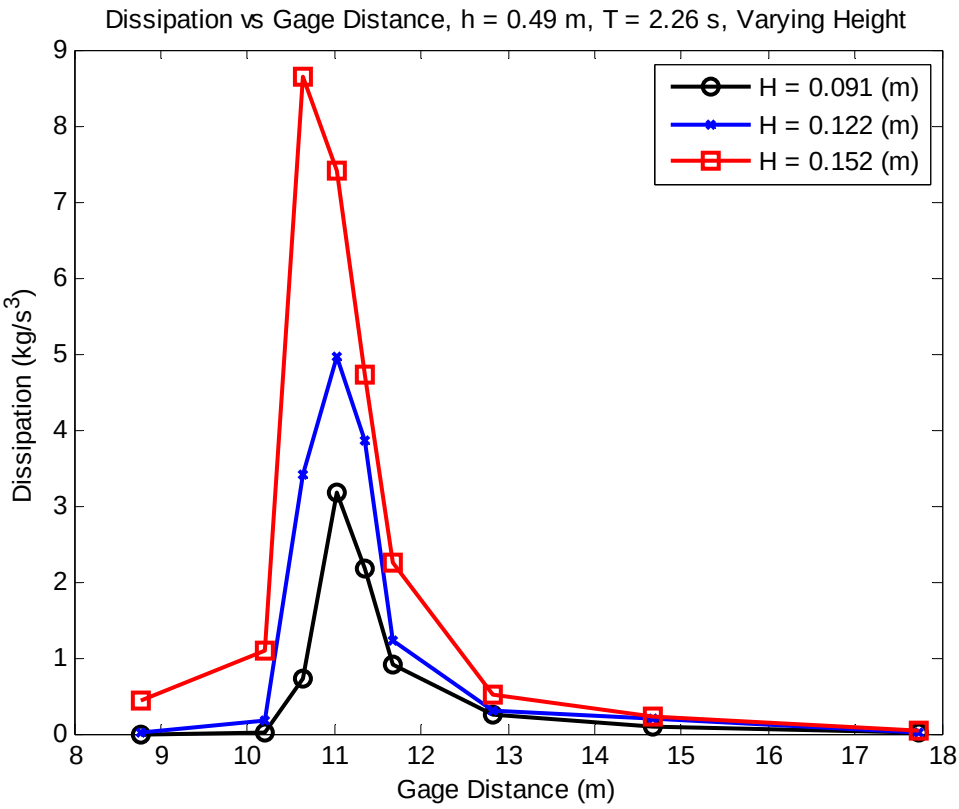

Figure 20: Low Frequency Dissipation vs. Gage Distance, Varying Incident Wave Height

When analyzing this along with Figure 21, the percentage of dissipation occurring in the low frequencies, we can note that at the beginning of the reef shelf, there is little dissipation occurring in the low frequencies in comparison to the total dissipation occurring at these locations. This implies that much of the long-wave energy will survive the breaking process and is allowed to penetrate the reef top.

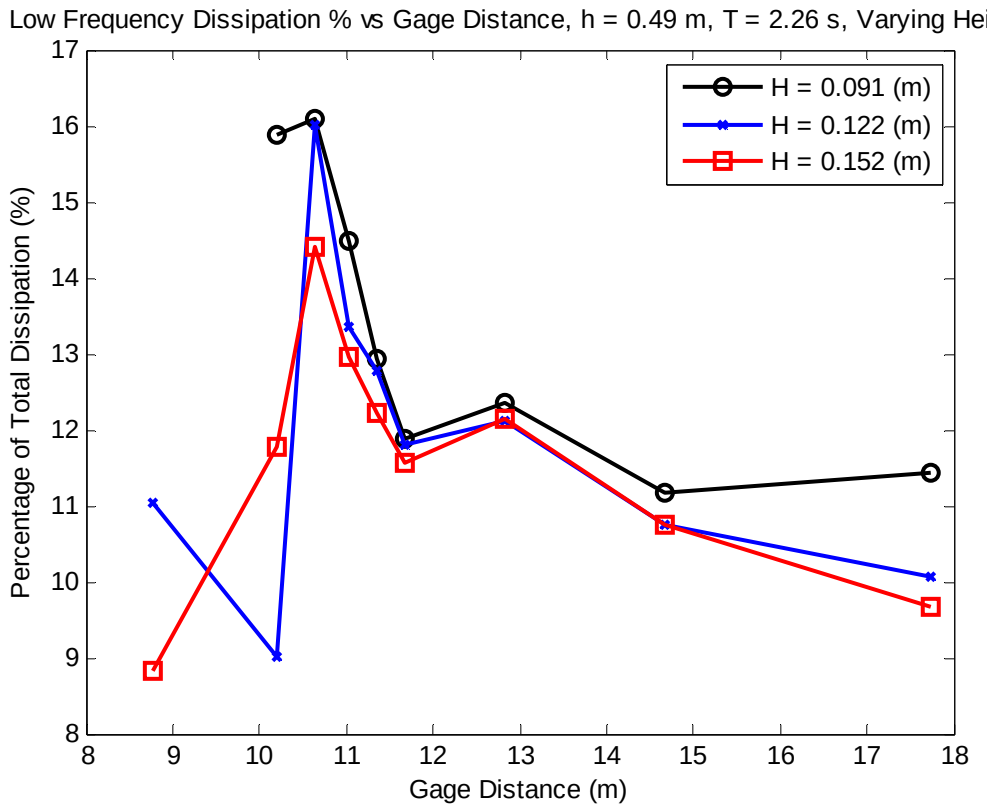

Figure 21: Percentage of Total Dissipation in Low Frequency, Varying Incident Wave Height

On the reef shelf we see that the amount of low frequency dissipation as part of the whole is even smaller. This further implies that much of the low frequency energy is not dissipating via breaking as it normally would, and allows for an increase in low-frequency energy on the reef shelf

B. Varying Incident Period

Variation of the incident wave period will change the distribution of the wave energy in the system, due to the larger or smaller peak frequency of the incoming waves. The effect of changing the wave period can be seen in Figure 22.

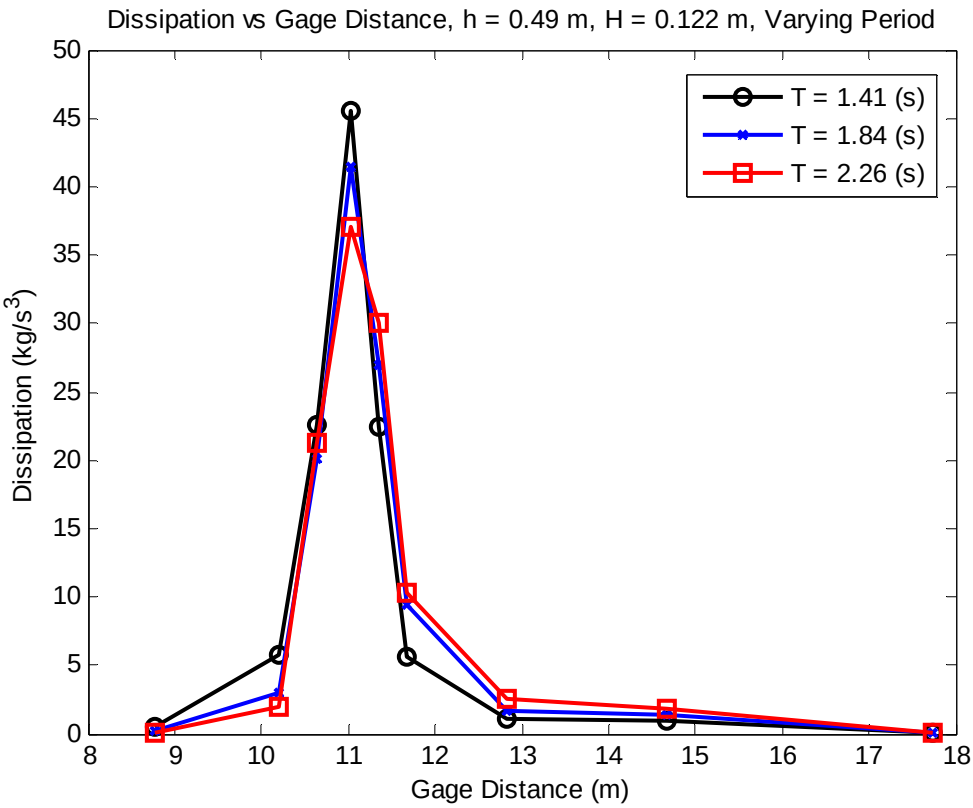

Figure 22: Total Dissipation vs. Gage Distance, Varying Incident Wave Period

Here we see that changes to the period do not cause much of an effect on the total dissipation in the entire system. The wave period does have a slight effect on the location of dissipation. Shorter period waves break earlier and more intense on the steep slope. Waves with a larger period still have the bulk of their breaking at gage seven, the toe of the reef shelf, but they experience less breaking and dissipation on the steep slope and up to this point of the reef, while showing in increase in dissipation on the reef shelf. Again, we analyze in finer detail the dissipation effects by looking at the low frequency band of waves, and see how it may vary in comparison to the bulk dissipation. The low-frequency dissipation versus period changes is shown in Figure 23.

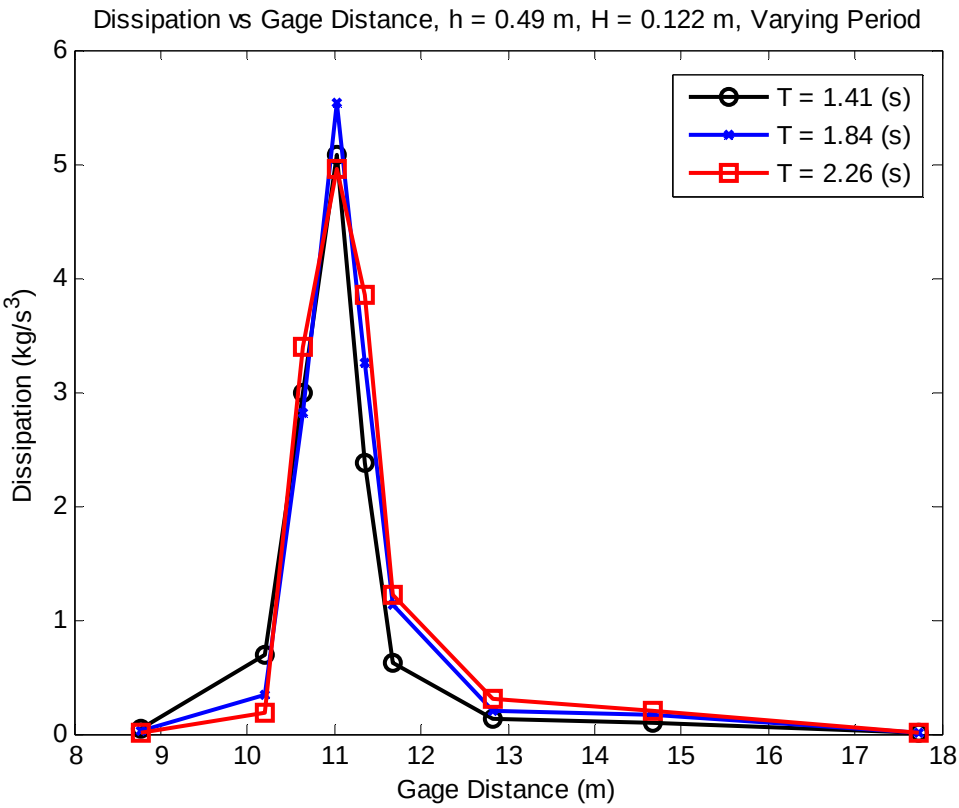

Figure 23: Low Frequency Dissipation vs. Gage Distance, Varying Incident Wave Period

From this figure we see that the long waves in the system follow the same pattern as that of the bulk dissipation. The lack of dissipation in the low frequency as part of the total dissipation can be seen in Figure 24. The amount of dissipation in the lower frequency range is a small amount compared to the total dissipation at the gages near the toe of the slope. We also see that this continues on the reef shelf.

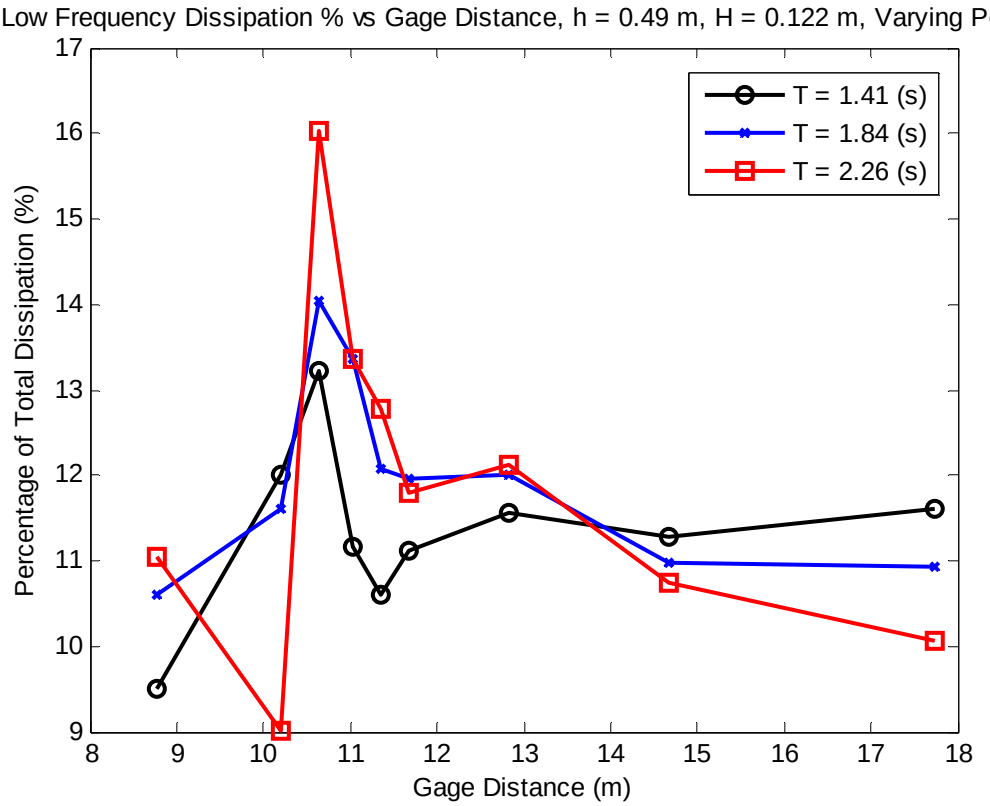

Figure 24: Percentage of Total Dissipation in Low Frequency, Varying Incident Wave Period

From this we can infer that on the shelf of the reef the low-frequency energy in the system is going to have a stronger influence due to the lack of dissipation in these locations in comparison to the amount of dissipation occurring at other frequencies.

C. Varying Water Depth

Changes in the water depth of the system do not have any effect on the amount of total energy in the system, as it makes no change to the incident wave conditions. However, it does have an effect on the location and amount of dissipation at each gage. This can be observed in Figure 25, where dissipation versus changing initial water depth is shown.

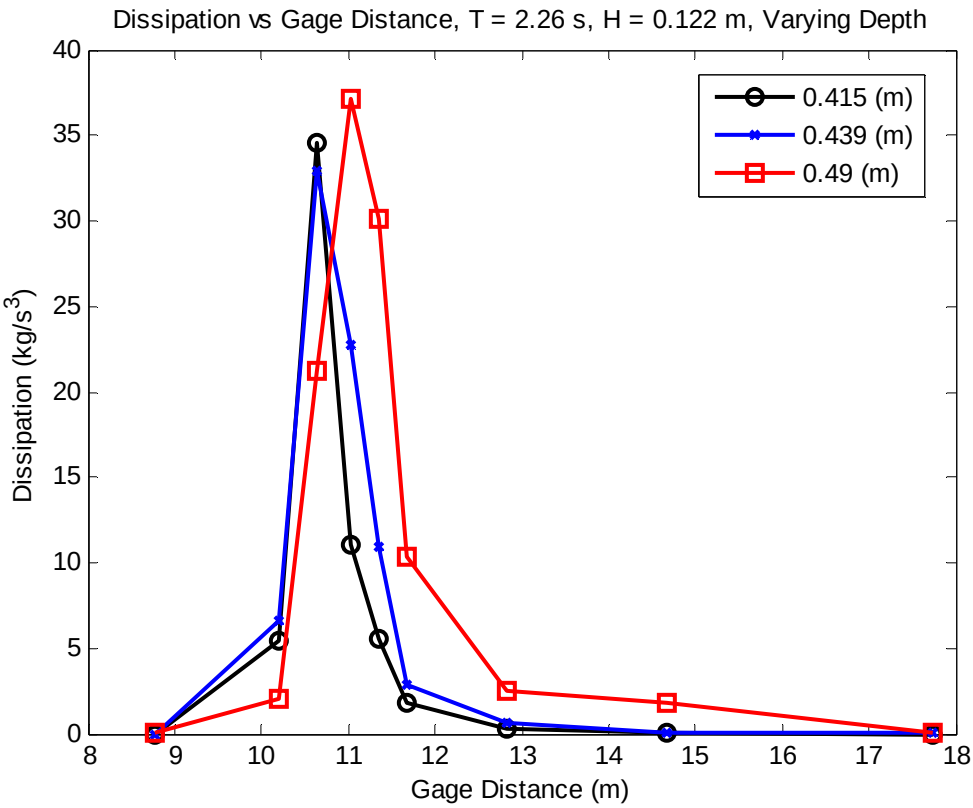

Figure 25: Total Dissipation vs. Gage Distance, Varying Water Depth

At the low and medium water depths, the most dissipation occurs at gage six, before the toe of the shelf, on the steep slope of the reef. At lower water depths we observe that waves are dissipating further offshore, resulting in less total energy making it to the shelf portion of the reef. This can be seen in Figure 26.

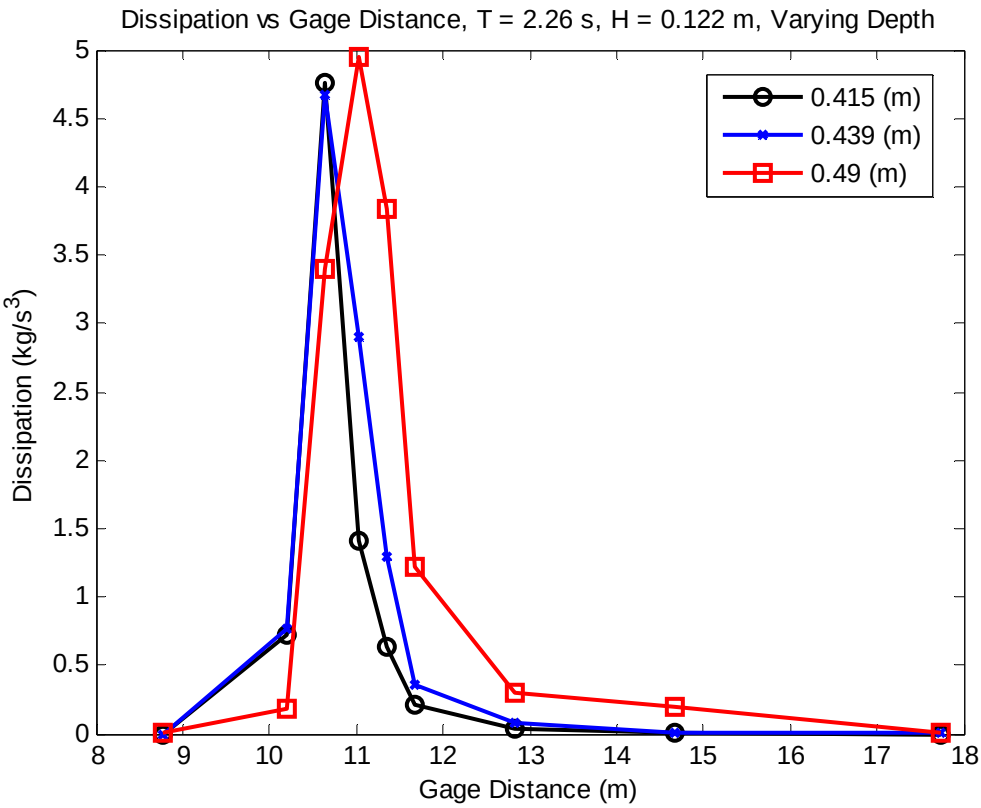

Figure 26: Low Frequency Dissipation vs. Gage Distance, Varying Depth

This also shows that though smaller depths move the breaking point and area of largest dissipation farther away from the toe of the shelf, the energy that is being dissipated at this location is in large part at higher frequencies, as seen in Figure 27 where the percentage of total dissipation in the low frequencies can is shown to be small. This allows low-frequency, long-waves to drive the effects on the shelf of the reef. However, as the water depth increases, more of the total dissipation consists of energy from the low-frequency bands, decreasing the influence of low energy on the reef shelf.

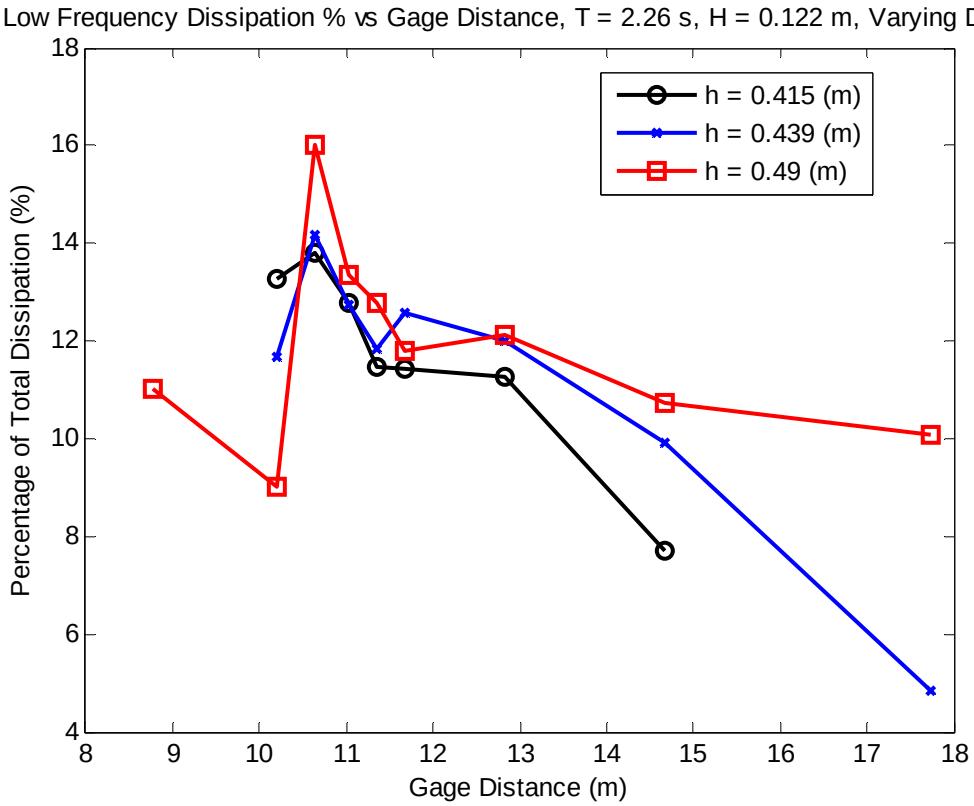

Figure 27: Percentage of Total Dissipation in Low Frequency, Varying Depth

D. Summation

From this analysis we are able to determine the effects of varying wave and water level conditions on long-wave energy and dissipation over a reef system. Changes to the incoming wave height will increase the total amount of energy, and thus dissipation, in the system. Though more dissipation occurs at the slope of the reef, much of the additional energy from the larger wave height reaches the shelf of the reef. However, this increase of dissipation on the slope of the reef does not increase the amount of long-

wave dissipation occurring to levels more than any other frequencies. The increase in dissipation is even across the range of frequencies seen in the system.

Variations in the period of incoming waves do not have any effect on the amount of total energy in the system or the location of the peak dissipation. This variation does have an effect on the amount of dissipation at each gage. Waves with a larger period will dissipate less energy on the slope of the reef, and waves with a smaller period dissipate more energy on the slope. The result is that longer period waves transmit more energy onto the shelf of the reef. In addition, due to a lack of low-frequency dissipation on the reef shelf, we can observe that a larger portion of the energy on the shelf is comprised of low-frequency energy.

Water level affects the location of the peak dissipation. Similar to changes in the period, lower water levels force more waves to break and dissipate energy at the slope of the reef. At these shallower water levels less energy is transmitted to the top of the reef shelf, while at deeper water levels more energy is evident on top of the reef. However, at the lower water levels a larger portion of the energy remaining on top of the reef is from long waves.

From these results of wave conditions on the reef system we can estimate where the largest amount of long-wave energy will be on the shelf of the reef. A wave set that exhibits a large wave height and a long period will result in the most overall energy on

the shelf of the reef. If the water level is sufficiently low enough, the majority of that energy will be low-frequency long waves.

CHAPTER VI

CONCLUSIONS

In this thesis we have investigated the use of probabilistic bulk dissipation models for use on a reef system. We found that no single existing model can accurately estimate dissipation over the entire reef structure. Instead a combination of two models must be used, one for the steep portion, and one for the mild slope reef top. These two probabilistic bulk dissipation models are those proposed by JB07 and TG83 respectively. Physical insight from the combined model analysis is limited by its reliance on distribution model weightings and the formulation in terms of bulk dissipation.

Further investigation into dissipation was done through the use of a frequency based method of dissipation calculation proposed by KK96. This method is based on a combination of the free surface elevation and the instantaneous eddy viscosity dissipation of the time series data, which is used to calculate the dissipation rate for the system. The overall bulk dissipation can then be determined from this dissipation rate using the method of KE11.

Using the combined probabilistic models for the reef system as a metric for dissipation, we were then able to compare these estimates to those from the frequency-based analysis, and find that the frequency-based method overestimates the total dissipation in the system. Through further use of the probabilistic models as a metric for the amount of

dissipation, we modified the eddy viscosity of Zelt (1991) by modifying a value normally held constant and creating a breaking parameter in the formulation, *k*. For the areas with a mild slope or small effect from bathymetry a value of 0.7 is used, and for the areas with the largest effect from bathymetry a value of 0.9 is used. These modifications account for the breaking of wave groups. The modification of this breaking limiter in the eddy viscosity has not been done before, and the use of it in this research shows that the modification of this parameter can be used in other applications to help account for excess dissipation normally found when using this model on non-solitary waves.

The frequency based analysis allows for the estimation of dissipation with no further reliance on probability distributions and corresponding weightings. A key feature of this method is it allows for analysis of wave energy effects in finer detail than bulk dissipation models allow. One advantage is the ability to inspect frequency dependent dissipation, particularly in the low-frequency range of the spectrum.

From this analysis we are able to determine the effects of not only bulk dissipation over the entire spectrum, but also long-wave dissipation for various wave conditions. Larger wave heights are found to have an overall increase on dissipation in the system, but do not affect long-wave dissipation. Longer wave periods result in less dissipation on the slope portion of the reef, and increased dissipation on the shelf portion. It also allows a slightly larger amount of long-wave energy to be transmitted to the shelf of the reef.

Shallower water depths appear to have the largest effect on the amount of long-wave energy on the shelf of the reef. When the water depths become small on the shelf of the reef we see that much energy in the system does not transmit to the shelf, however what energy does transmit consists mostly of long-wave energy.

The frequency-based dissipation analysis is a flexible tool that allows insight into dissipative effects. The ability to analyze not only bulk dissipation, but dissipation at different frequencies is a powerful tool in discovering the effects of waves on unique beach and shoreline systems. Future work in this area will involve further investigation of the linkage between the dissipation rate and the free surface spectrum, including parameterization of the links between the slope of the spectral tail and wave breaking. Further study is also to be performed into developing probability distribution functions of the instantaneous dissipation rates for use in numerical models of wave breaking.

REFERENCES

Battjes, J.A., and J.P.F.M. Janssen. 1978. Energy Loss and Set-up Due to Breaking of Random Waves, *Proceedings of 16th International Conference on Coastal Engineering*, Hamburg, Germany, ASCE, 466-480.

Battjes, J.A., and M.J.F. Stive. 1985. Calibration and Verification of a Dissipation Model for Random Breaking Waves, *Journal of Geophysical Research*, 90 (C5), 9159-9167.

Baldock, T.E., P. Holmes, S. Bunker, P. and Van Weert. 1998. Cross-shore Hydrodynamics within an Unsaturated Surf Zone, *Coastal Engineering*, 34, 173-196.

Chen, Y., Guza, R.T. and Elgar, S. 1997. Modeling Spectra of Breaking Surface Waves in Shallow Water, *Journal for Geophysical Research,* 102 (C11), 25035-25046.

Janssen, T.T., and J.A. Battjes. 2007. A Note on Wave Energy Dissipation Over Steep Beaches, *Coastal Engineering*, 54, 711-716.

Kaihatu, J.M., and H.M. El Safty. 2011. Spectral Description of Energy Dissipation in Breaking Wave Groups, *Proceedings of 32nd International Conference on Coastal Engineering*, Shanghai, China, Waves 19.

Kaihatu, J.M., and Kirby, J.T. 1995. Nonlinear Transformation of Waves in Finite Water Depth. *Physics of Fluids*, 7, 1903-1914.

Kaihatu, J.M., J. Veeramony, K.L. Edwards, and J.T. Kirby. 2007. Asymptotic Behavior of Frequency and Wave Number Spectra of Nearshore Shoaling and Breaking Waves. *Journal of Geophysical Research*, 112, doi: 10.1029/2006JC003817.

Kirby, J.T., and J.M. Kaihatu. 1996. Structure of Frequency Domain Models for Random Wave Breaking, *Proceedings of 25th International Conference on Coastal Engineering*, Orlando, Florida, ASCE, 1144-1155.

Sverdrup, K.A., A.C. Duxbury, and A.B. Duxbury. 2005. *An Introduction to the World's Oceans*, McGraw-Hill, New York, New York, 107-110 pp.

Thornton, E.B., and R.T. Guza. 1983. Transformation of Wave Height Distribution, *Journal of Geophysical Research*, 88, 5925-5938.

Zelt, J.A. 1991. The Run-up of Nonbreaking and Breaking Solitary Waves. *Coastal Engineering*, 15,205-246.

APPENDIX A

EXPERIMENTAL RUNS

Table A - 1: 1:5 Slope Reef Runs

Run	Model T_p (sec)	Model H_i (m)	Model d (m)	Reef Slope
102	2.83	0.122	0.49	1:5
104	2.26	0.091	0.49	1:5
105	2.26	0.122	0.49	1:5
106	2.26	0.152	0.49	1:5
107	1.84	0.091	0.49	1:5
108	1.84	0.152	0.49	1:5
111	1.41	0.091	0.49	1:5
112	1.84	0.104	0.49	1:5
113	1.41	0.104	0.49	1:5
114	1.41	0.140	0.49	1:5
115	0.99	0.104	0.49	1:5
116	0.99	0.079	0.49	1:5
117	0.99	0.098	0.44	1:5
119	0.99	0.079	0.44	1:5
120	1.41	0.134	0.44	1:5
122	1.41	0.116	0.44	1:5
123	1.41	0.073	0.44	1:5
126	2.26	0.146	0.44	1:5
127	2.83	0.159	0.44	1:5
128	1.84	0.152	0.44	1:5
129	1.84	0.085	0.44	1:5
130	1.84	0.122	0.44	1:5
131	2.26	0.091	0.44	1:5
134	2.26	0.122	0.44	1:5
135	2.83	0.085	0.44	1:5
136	2.83	0.122	0.44	1:5
137	2.83	0.140	0.44	1:5
138	0.99	0.104	0.42	1:5
139	1.41	0.134	0.42	1:5
142	1.41	0.116	0.42	1:5
143	1.41	0.085	0.42	1:5
145	0.99	0.085	0.42	1:5
146	1.84	0.146	0.42	1:5
147	1.84	0.122	0.42	1:5
149	1.84	0.110	0.42	1:5
151	2.83	0.159	0.42	1:5
152	2.26	0.140	0.42	1:5
159	2.26	0.110	0.42	1:5
160	2.26	0.122	0.42	1:5
161	2.83	0.122	0.42	1:5
162	2.83	0.104	0.42	1:5

APPENDIX B

H_{RMS} COMPARISONS

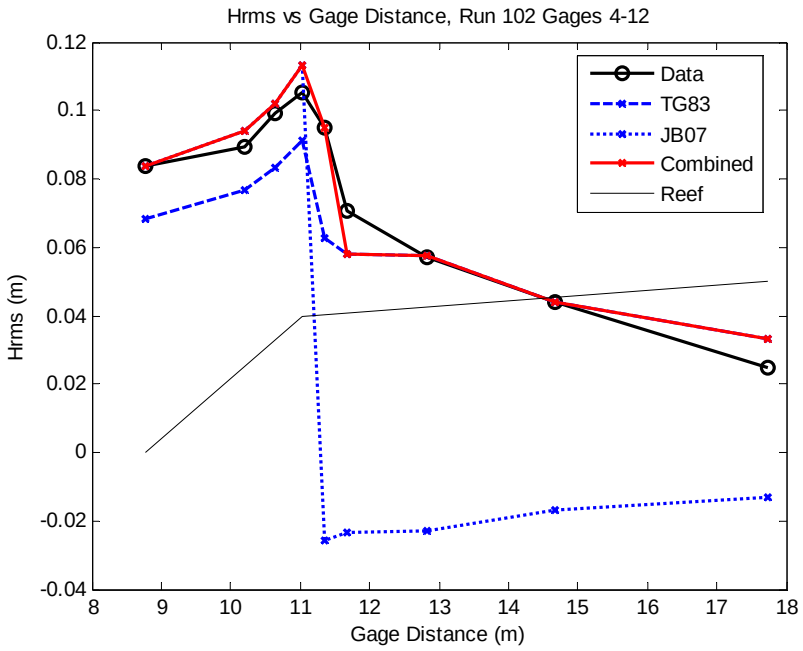

Figure B - 1: Model HRMS Compared to Measured Data, Run 102

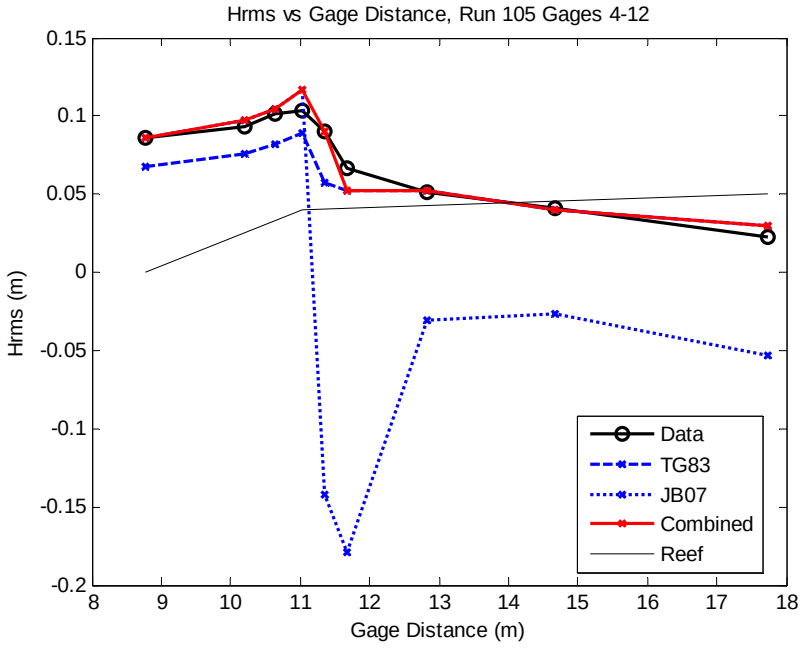

Figure B - 2: Model HRMS Compared to Measured Data, Run 105

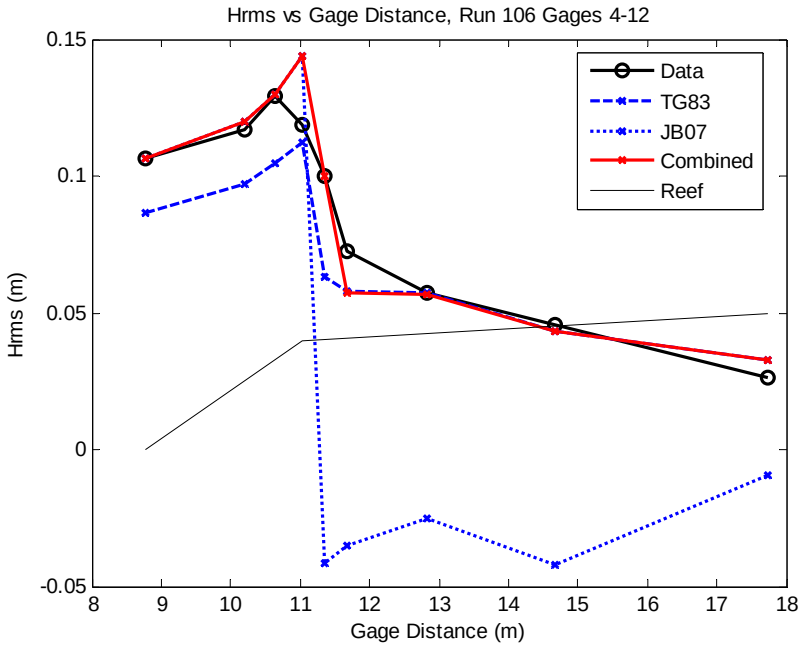

Figure B - 3: Model HRMS Compared to Measured Data, Run 106

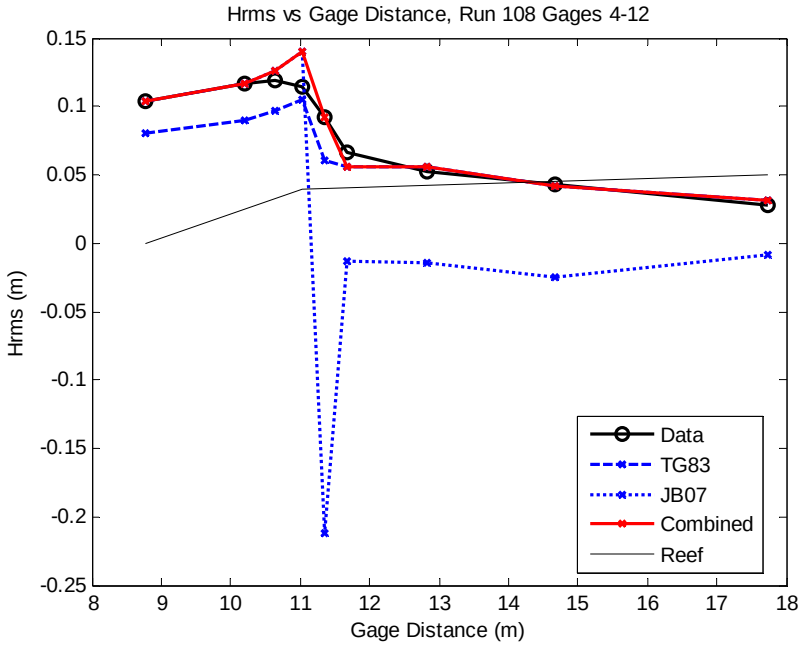

Figure B - 4: Model HRMS Compared to Measured Data, Run 108

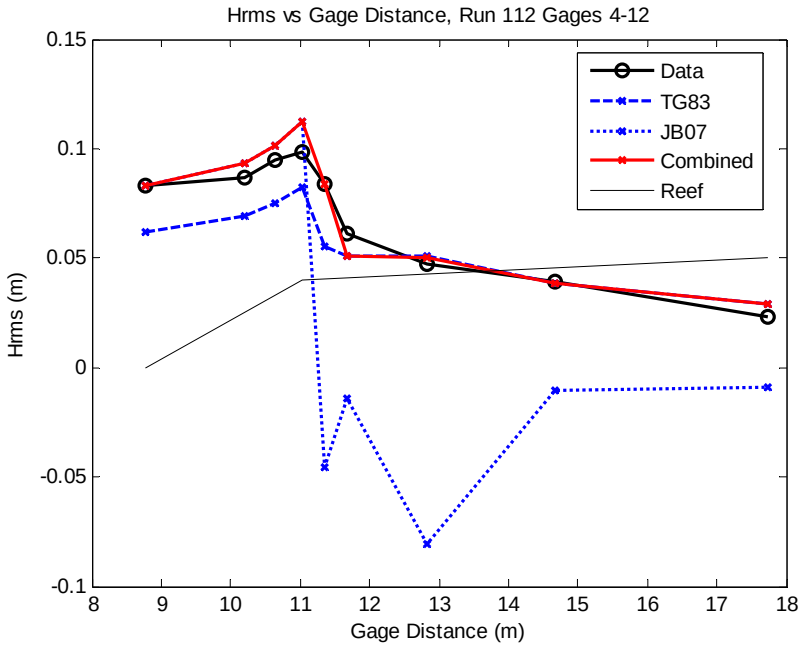

Figure B - 5: Model HRMS Compared to Measured Data, Run 112

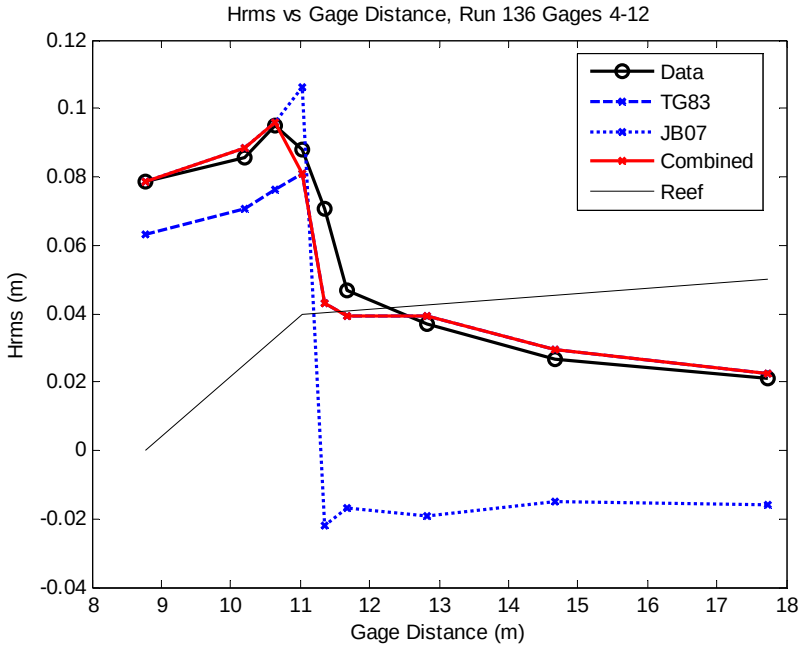

Figure B - 6: Model HRMS Compared to Measured Data, Run 136

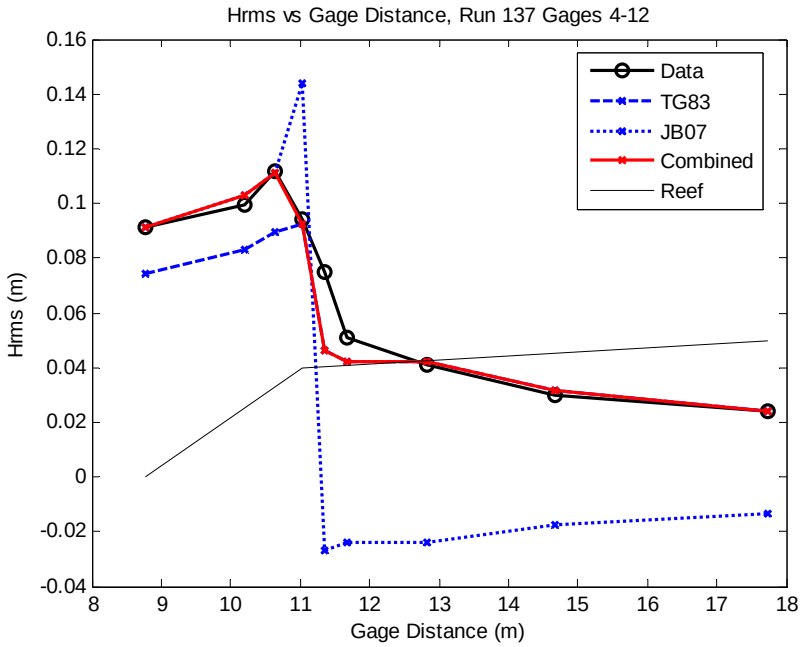

Figure B - 7: Model HRMS Compared to Measured Data, Run 137

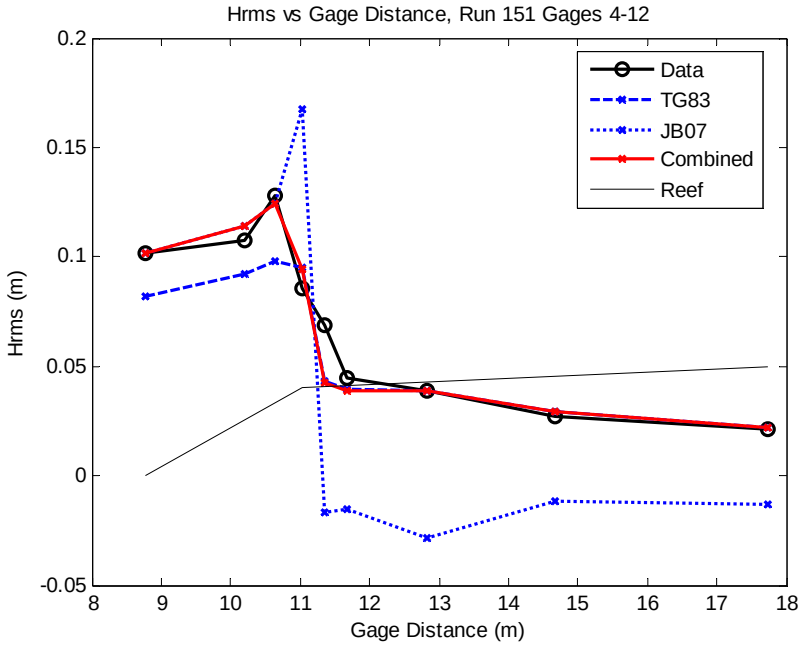

Figure B - 8: Model HRMS Compared to Measured Data, Run 151

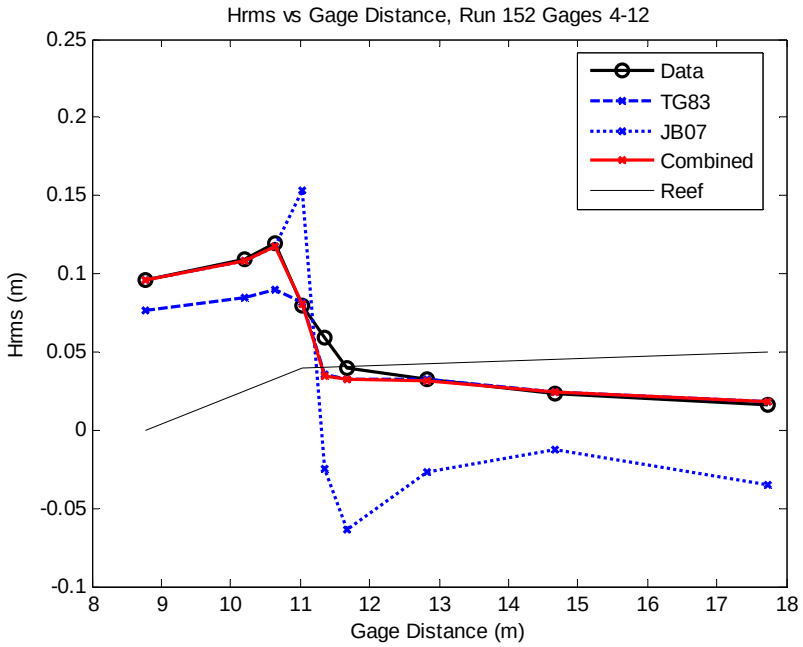

Figure B - 9: Model HRMS Compared to Measured Data, Run 152

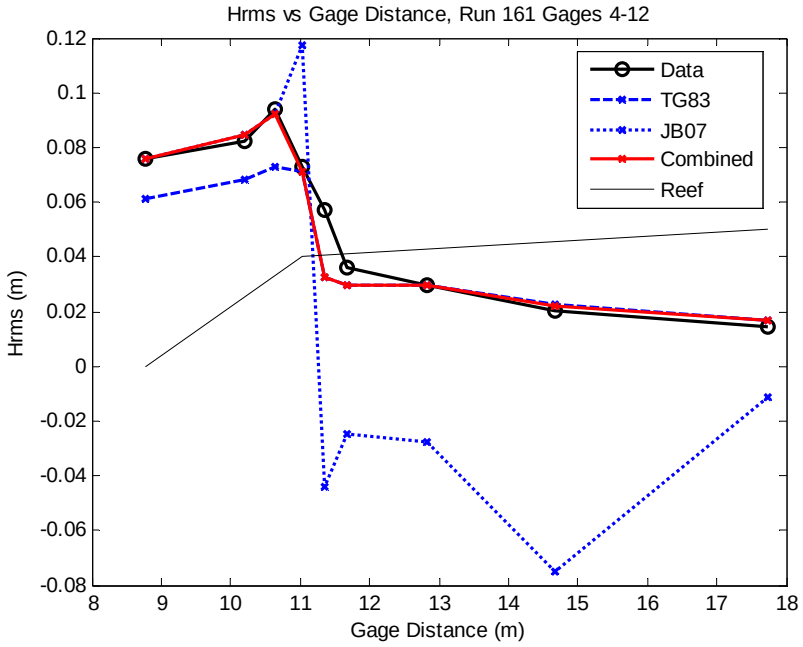

Figure B - 10: Model HRMS Compared to Measured Data, Run 161

APPENDIX C

DISSIPATION COMPARISONS

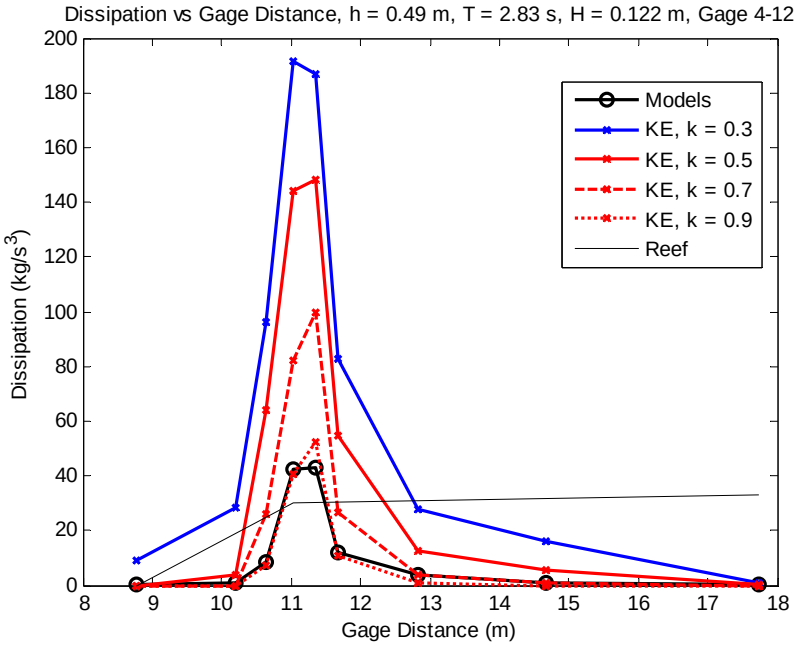

Figure C - 1: Frequency Based and Modeled Dissipation vs. Gage Distance, Varied *k*, Run 102

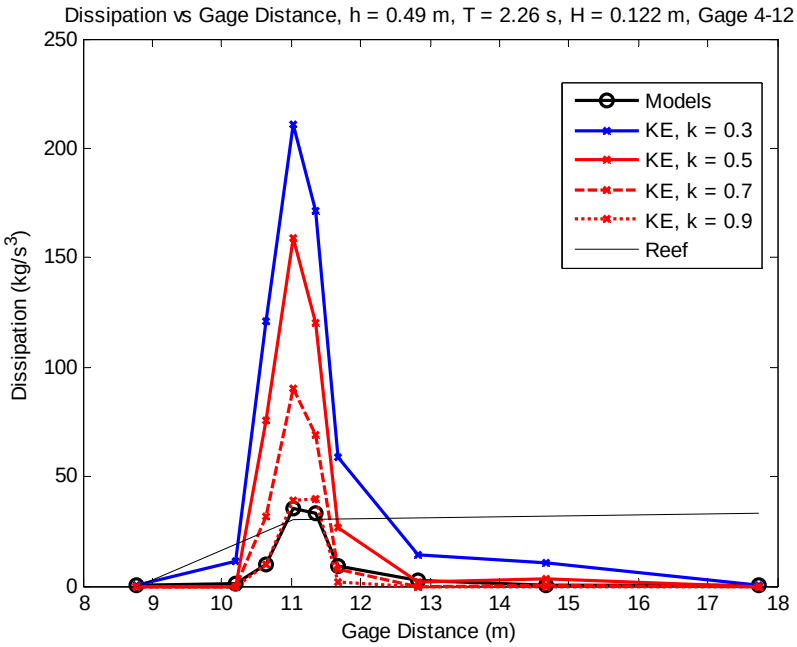

Figure C - 2: Frequency Based and Modeled Dissipation vs. Gage Distance, Varied *k*, Run 105

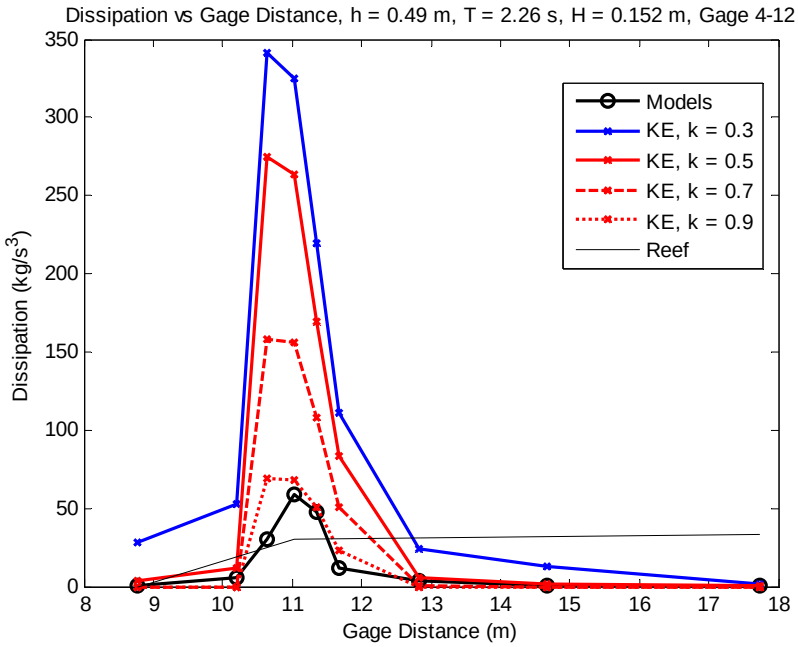

Figure C - 3: Frequency Based and Modeled Dissipation vs. Gage Distance, Varied *k*, Run 106

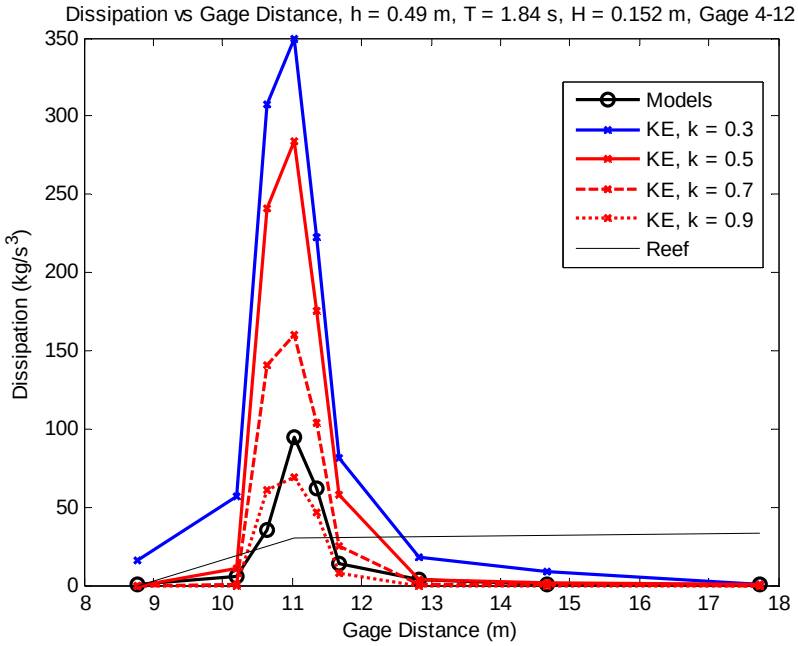

Figure C - 4: Frequency Based and Modeled Dissipation vs. Gage Distance, Varied *k*, Run 108

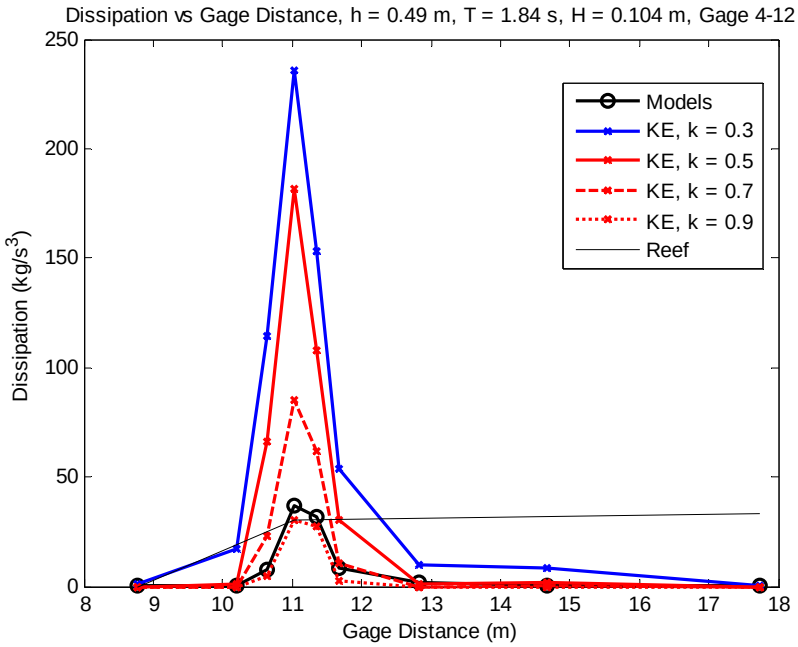

Figure C - 5: Frequency Based and Modeled Dissipation vs. Gage Distance, Varied *k*, Run 112

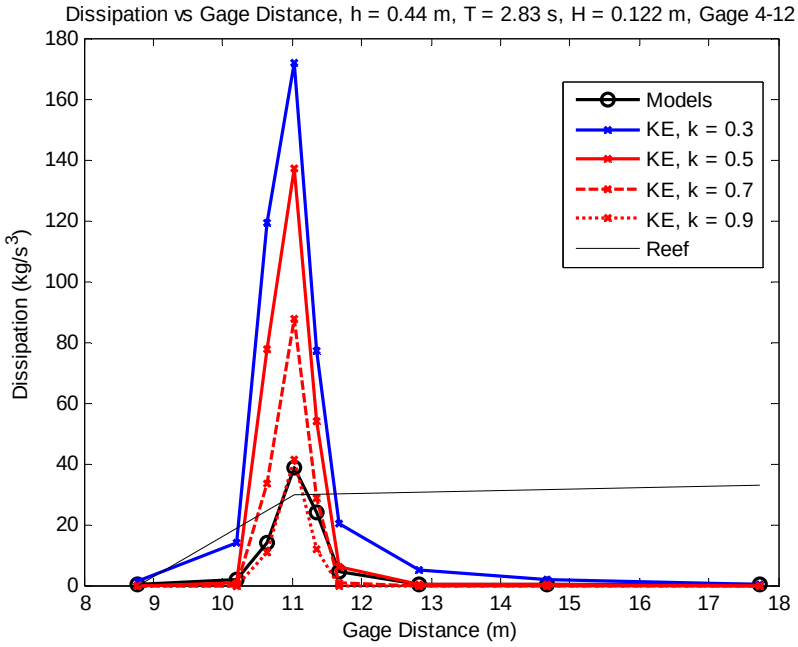

Figure C - 6: Frequency Based and Modeled Dissipation vs. Gage Distance, Varied *k*, Run 136

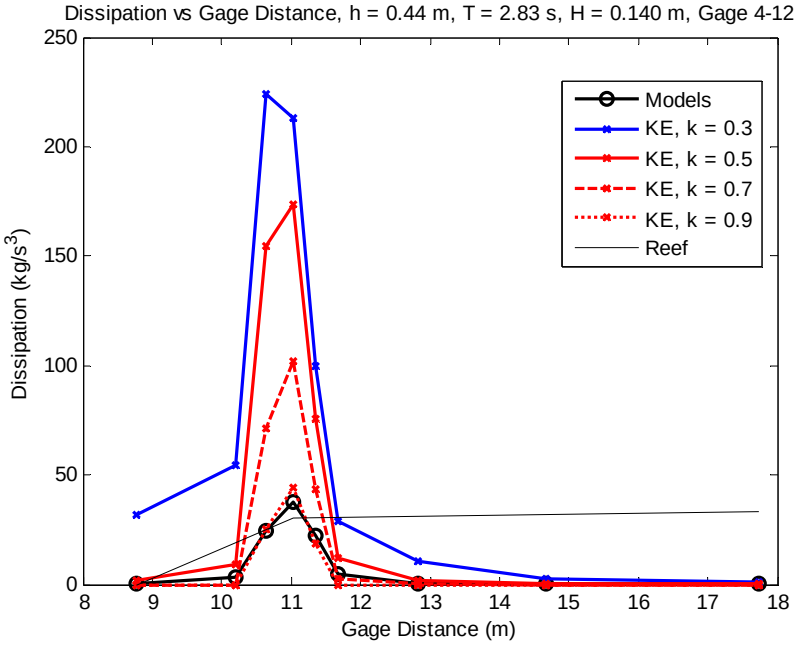

Figure C - 7: Frequency Based and Modeled Dissipation vs. Gage Distance, Varied *k*, Run 137

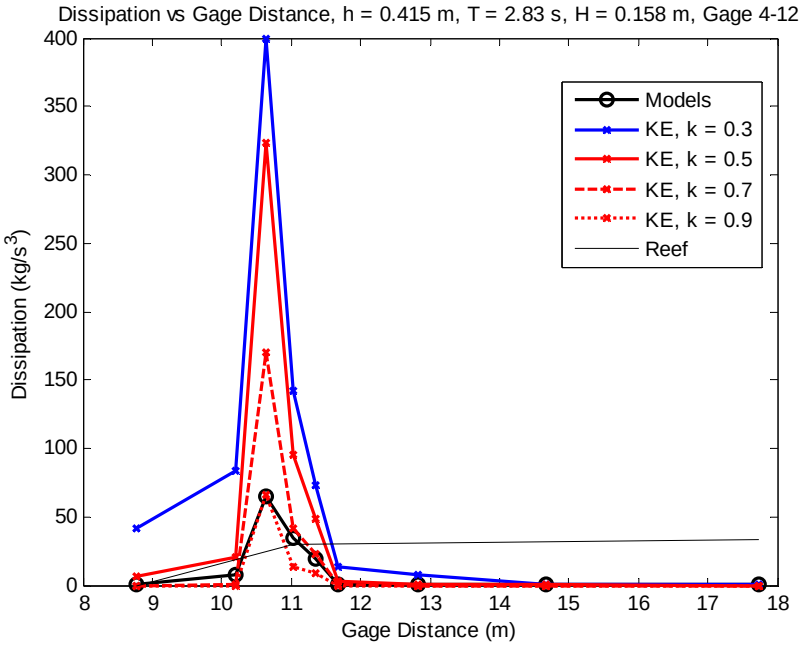

Figure C - 8: Frequency Based and Modeled Dissipation vs. Gage Distance, Varied *k*, Run 151

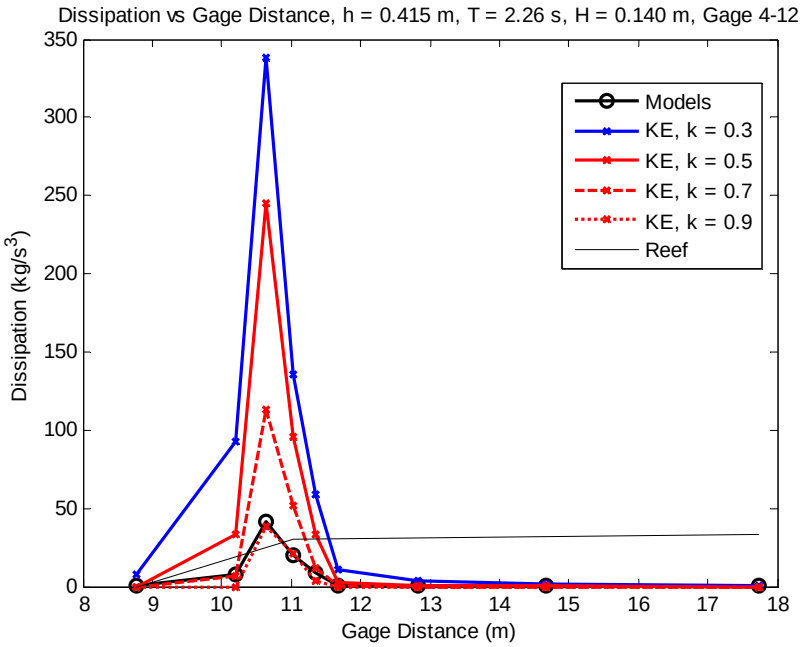

Figure C - 9: Frequency Based and Modeled Dissipation vs. Gage Distance, Varied *k*, Run 152

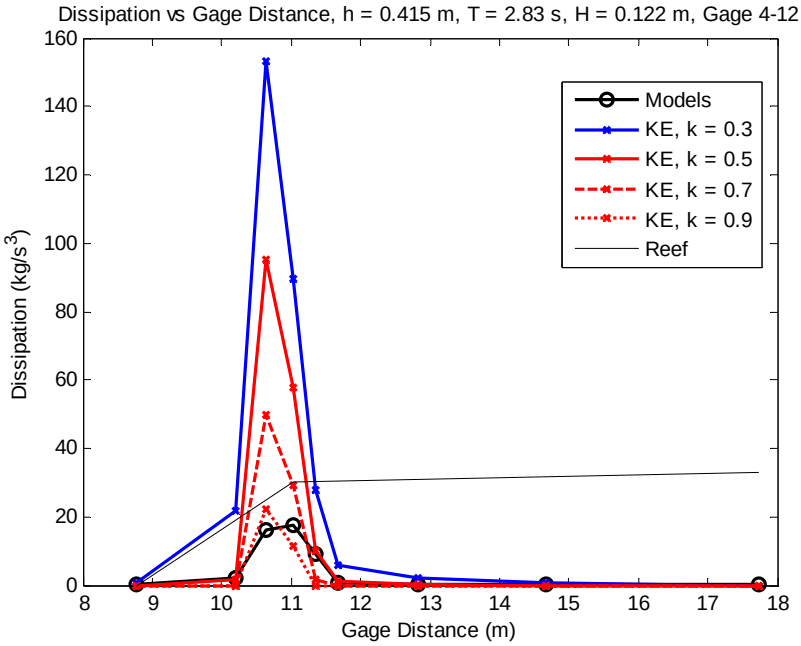

Figure C - 10: Frequency Based and Modeled Dissipation vs. Gage Distance, Varied *k*, Run 161

APPENDIX D

WAVE CONDITION COMPARISONS

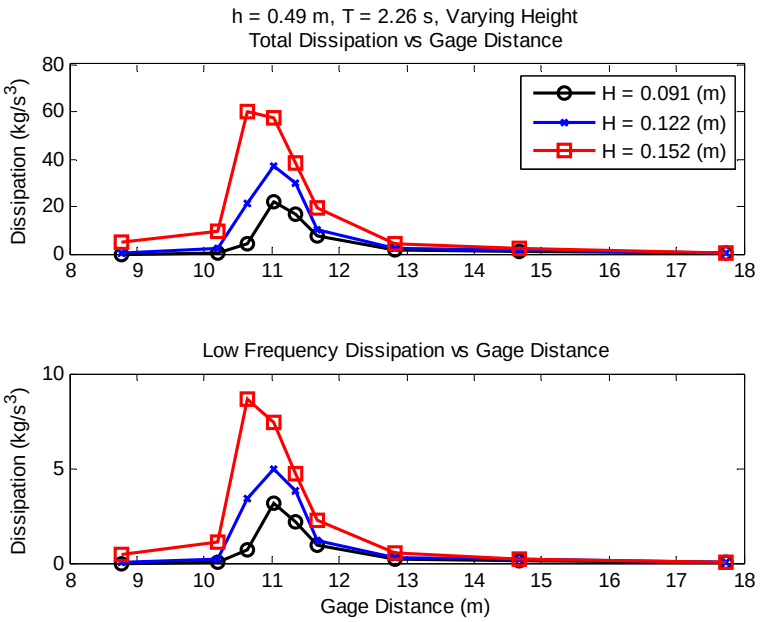

Figure D - 1: Total and Low Frequency Dissipation vs. Gage Locations; Varying Incident Wave Height; Runs 104, 105, 106

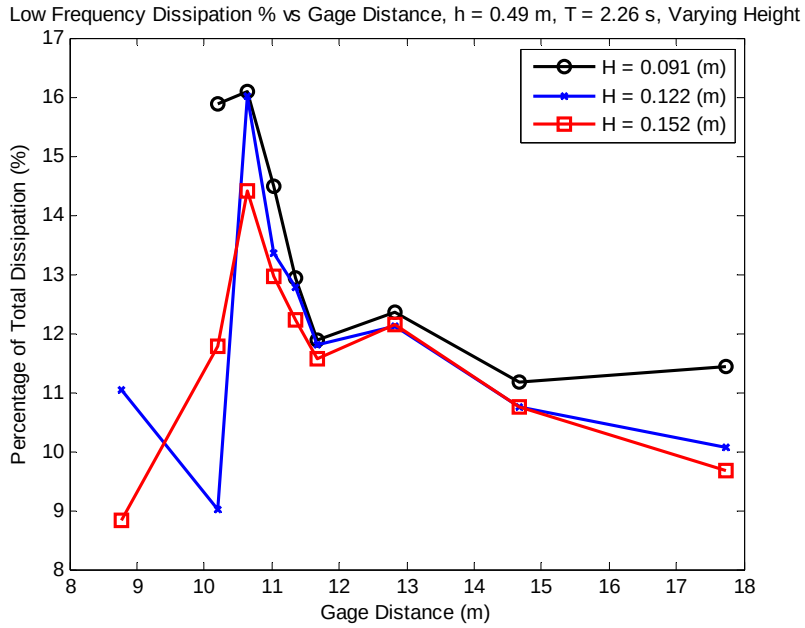

Figure D - 2: Percentage of Total Dissipation Occurring in Low Frequencies; Varying Incident Wave Height; Runs 104, 105, 106

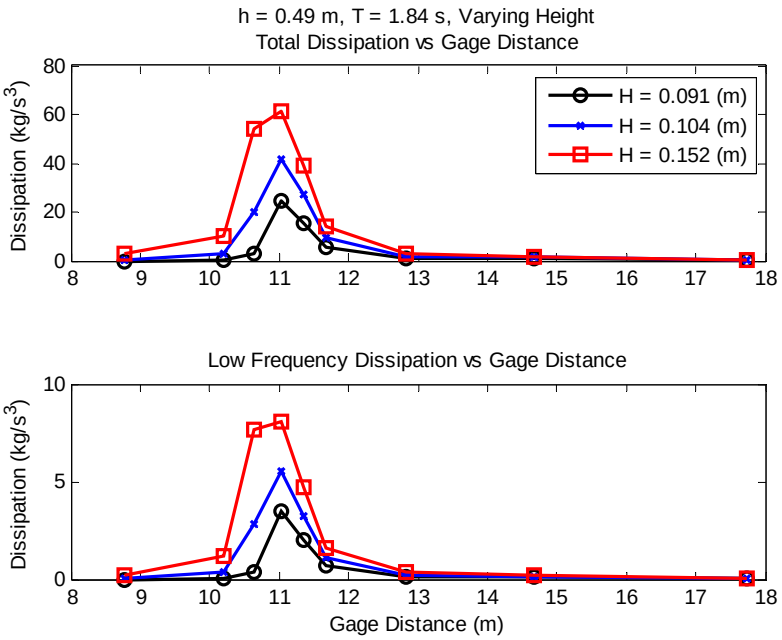

Figure D - 3: Total and Low Frequency Dissipation vs. Gage Locations; Varying Incident Wave Height; Runs 107, 112, 108

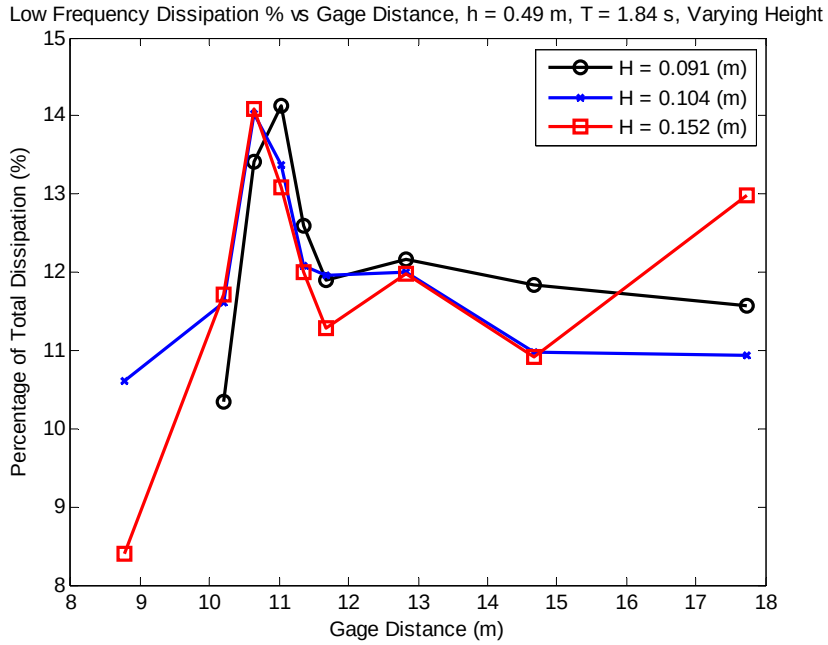

Figure D - 4: Percentage of Total Dissipation Occurring in Low Frequencies; Varying Incident Wave Height; Runs 107, 112, 108

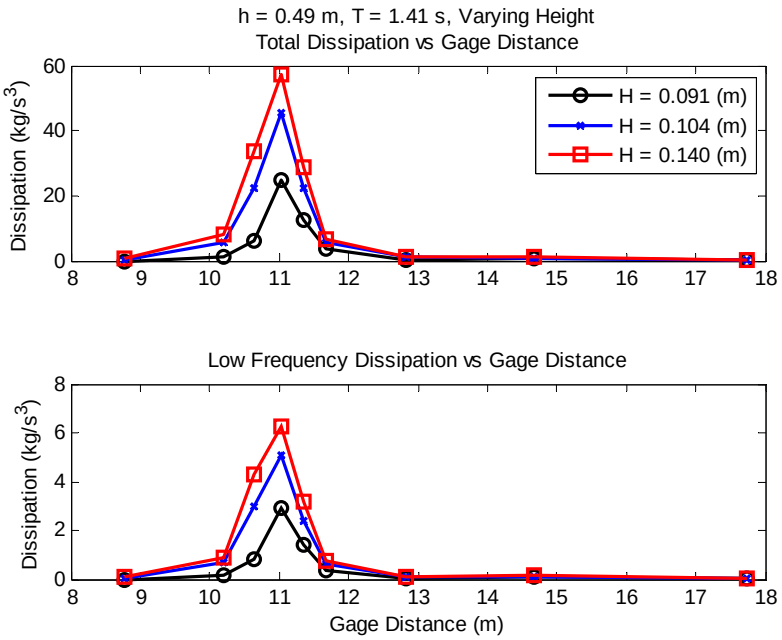

Figure D - 5: Total and Low Frequency Dissipation vs. Gage Locations; Varying Incident Wave Height; Runs 111, 113, 114

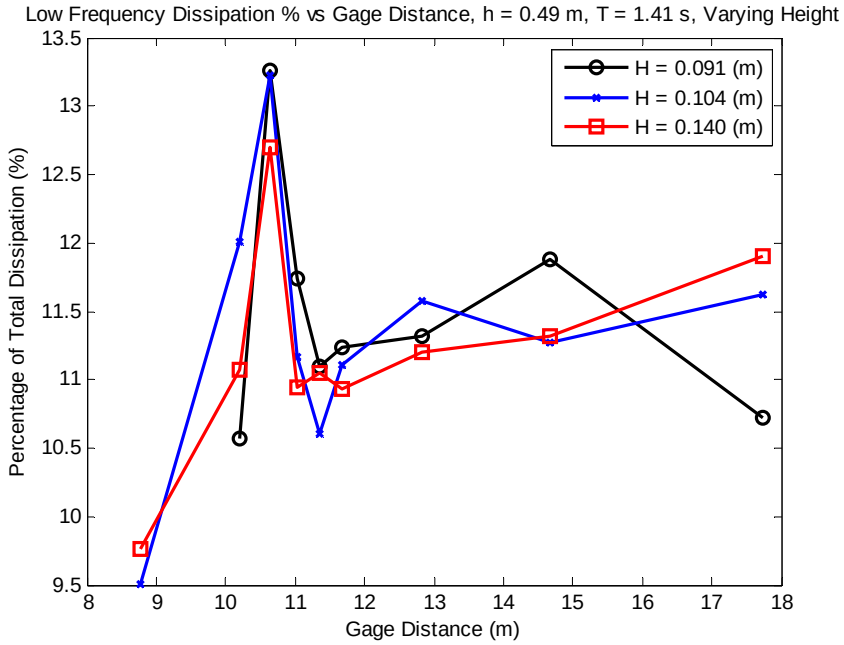

Figure D - 6: Percentage of Total Dissipation Occurring in Low Frequencies; Varying Incident Wave Height; Runs 111, 113, 114

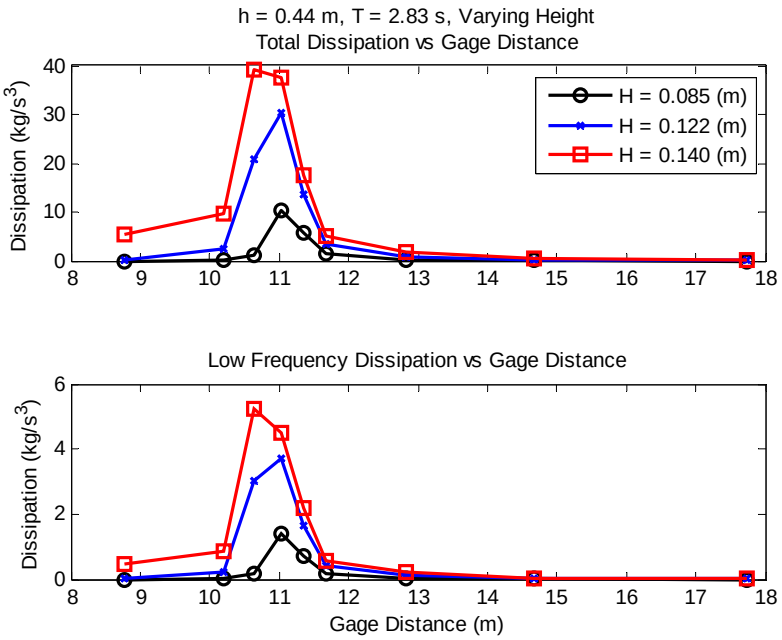

Figure D - 7: Total and Low Frequency Dissipation vs. Gage Locations; Varying Incident Wave Height; Runs 135, 136, 137

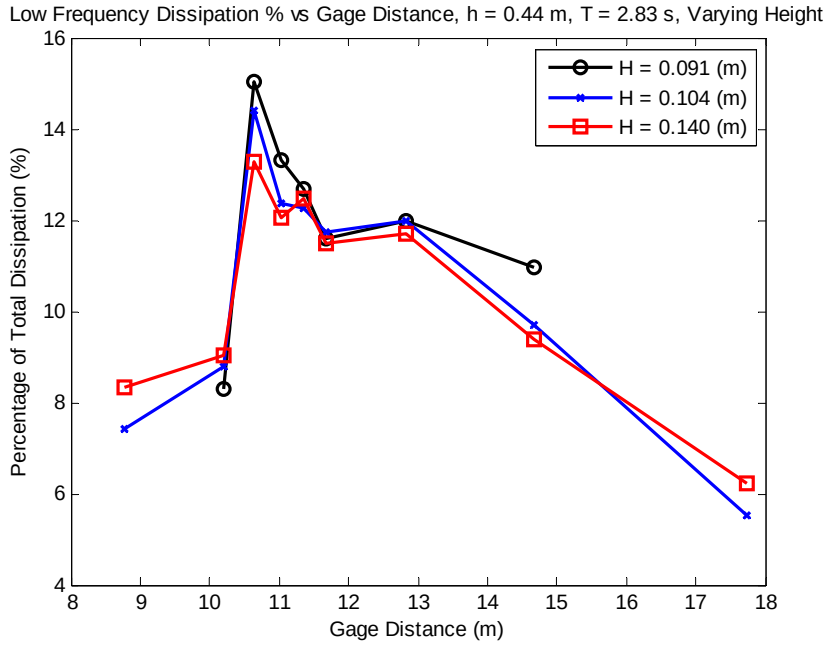

Figure D - 8: Percentage of Total Dissipation Occurring in Low Frequencies; Varying Incident Wave Height; Runs 135, 136, 137

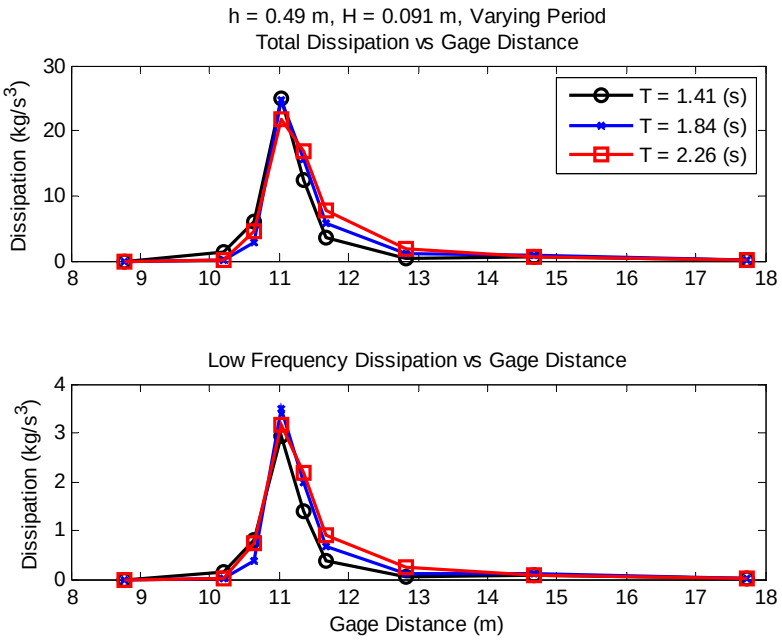

Figure D - 9: Total and Low Frequency Dissipation vs. Gage Locations; Varying Incident Period; Runs 111, 107, 104

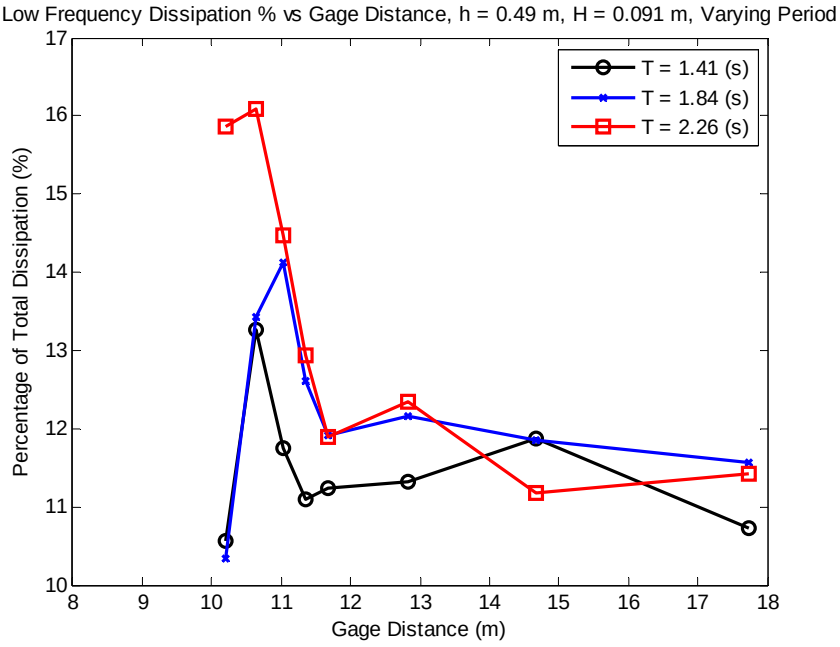

Figure D - 10: Percentage of Total Dissipation Occurring in Low Frequencies; Varying Incident Period; Runs 111, 107, 104

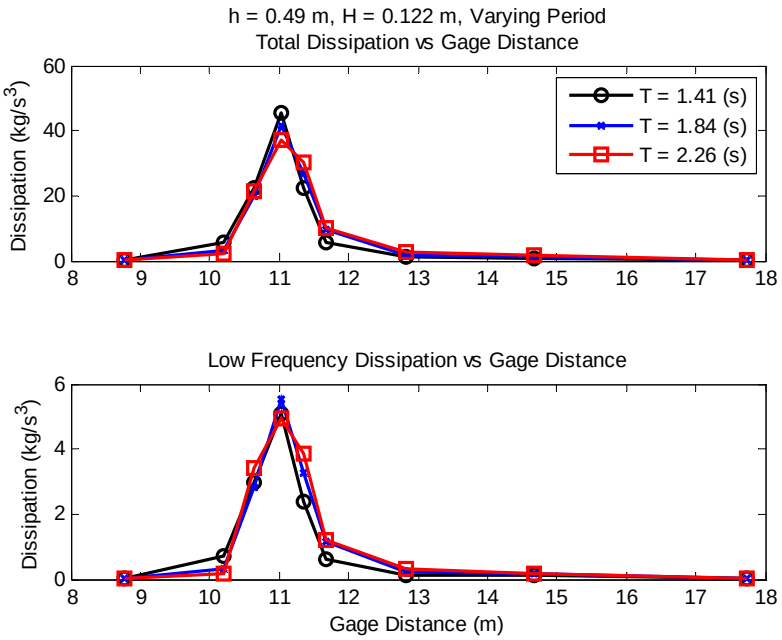

Figure D - 11: Total and Low Frequency Dissipation vs. Gage Locations; Varying Incident Period; Runs 113, 112, 105

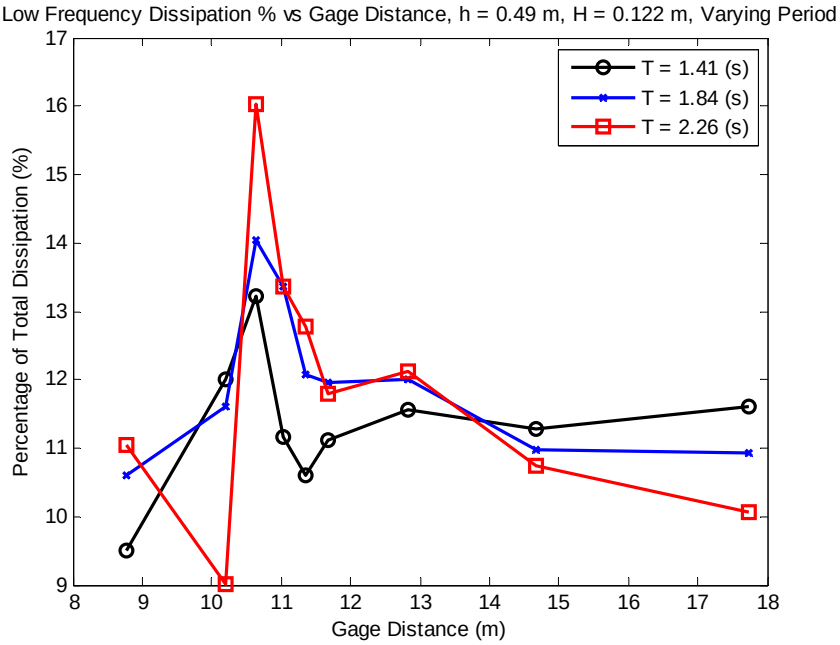

Figure D - 12: Percentage of Total Dissipation Occurring in Low Frequencies; Varying Incident Period; Runs 113, 112, 105

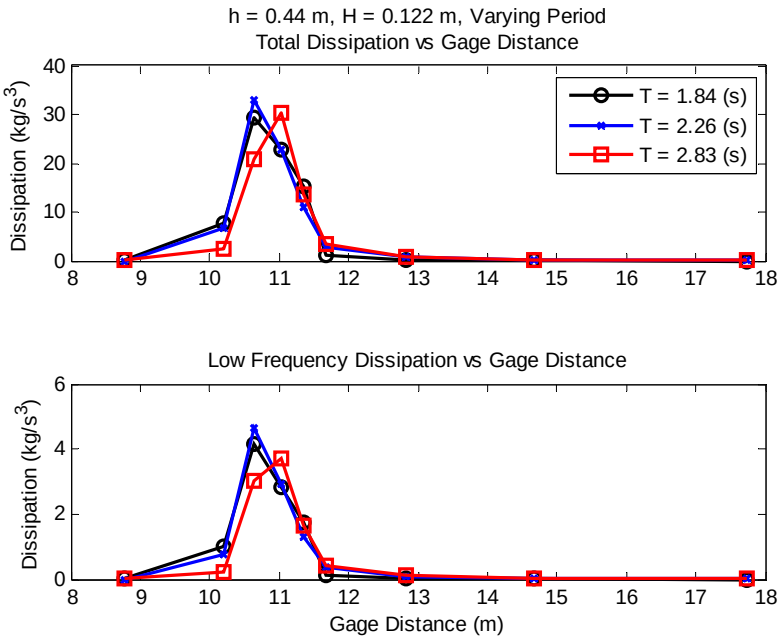

Figure D - 13: Total and Low Frequency Dissipation vs. Gage Locations; Varying Incident Period; Runs 130, 134, 136

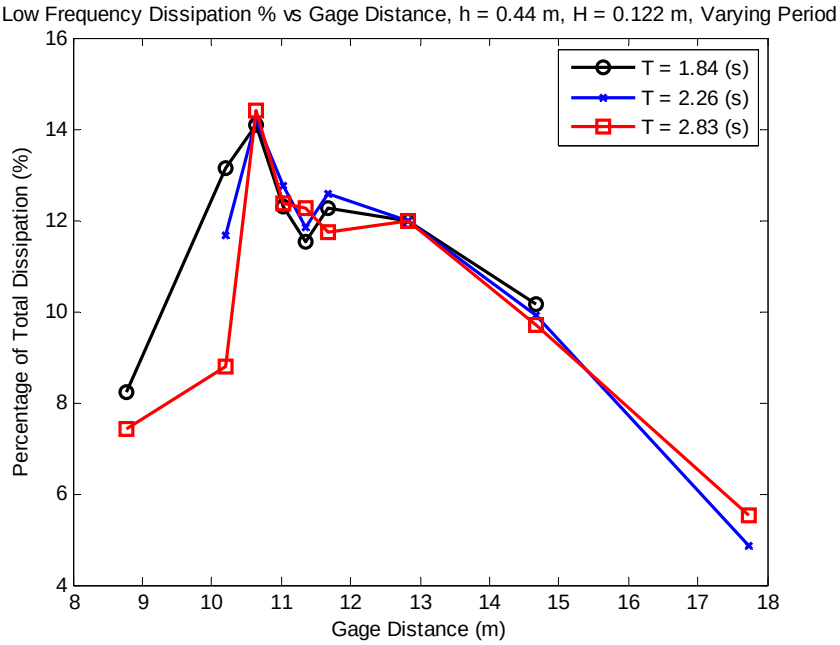

Figure D - 14: Percentage of Total Dissipation Occurring in Low Frequencies; Varying Incident Period; Runs 130, 134, 136

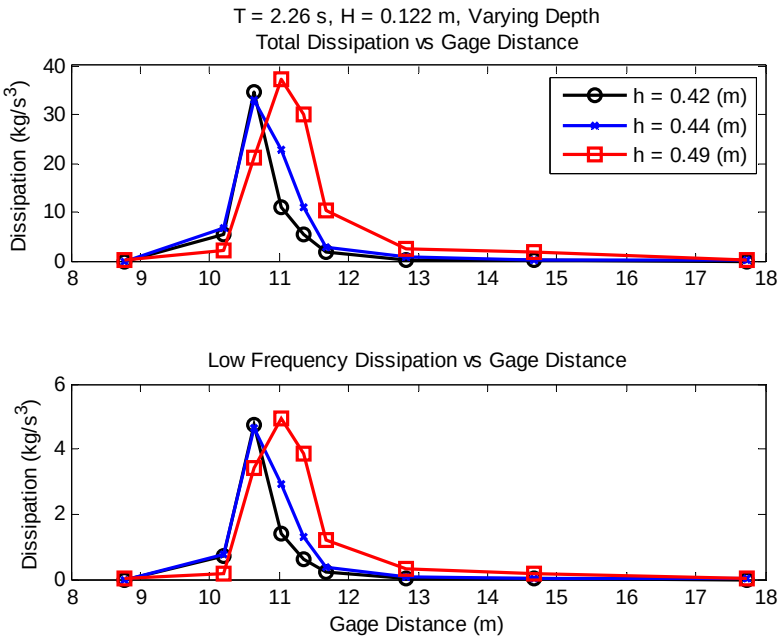

Figure D - 15: Total and Low Frequency Dissipation vs. Gage Locations; Varying Depth; Runs 160, 134, 105

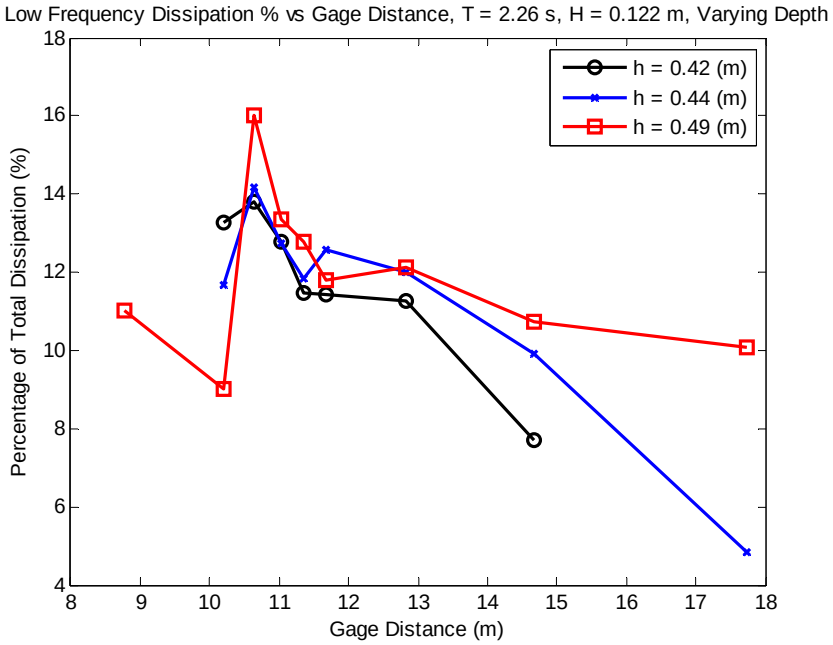

Figure D - 16: Percentage of Total Dissipation Occurring in Low Frequencies; Varying Depth; Runs 160, 134, 105

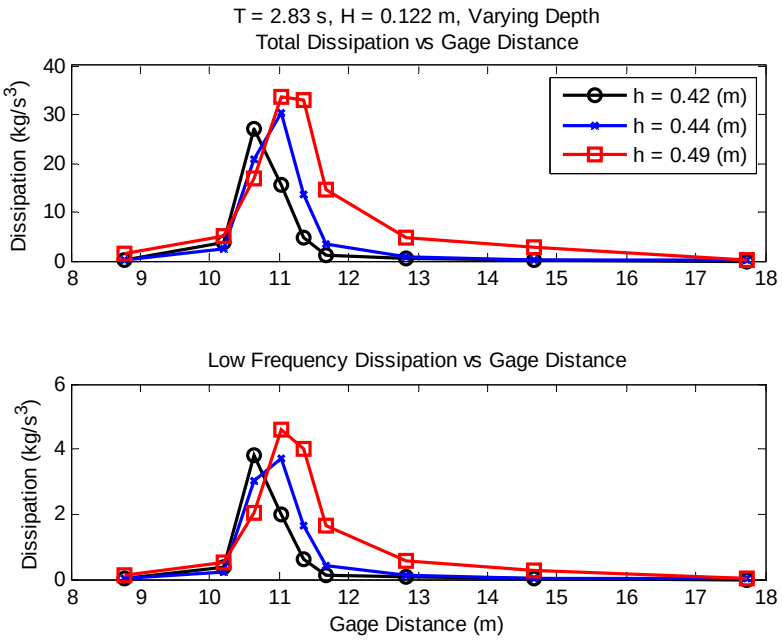

Figure D - 17: Total and Low Frequency Dissipation vs. Gage Locations; Varying Depth; Runs 161, 136, 102

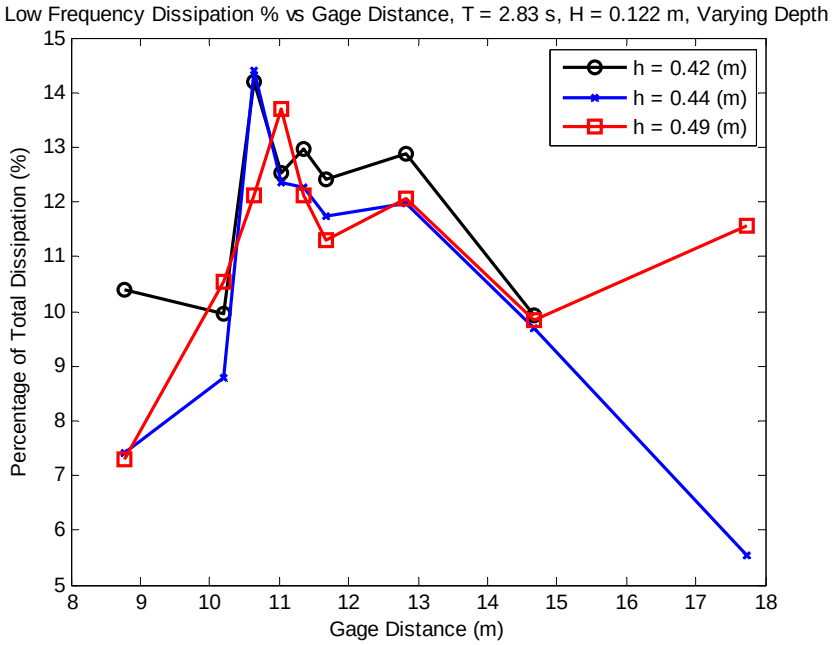

Figure D - 18: Percentage of Total Dissipation Occurring in Low Frequencies; Varying Depth; Runs 161, 136, 102

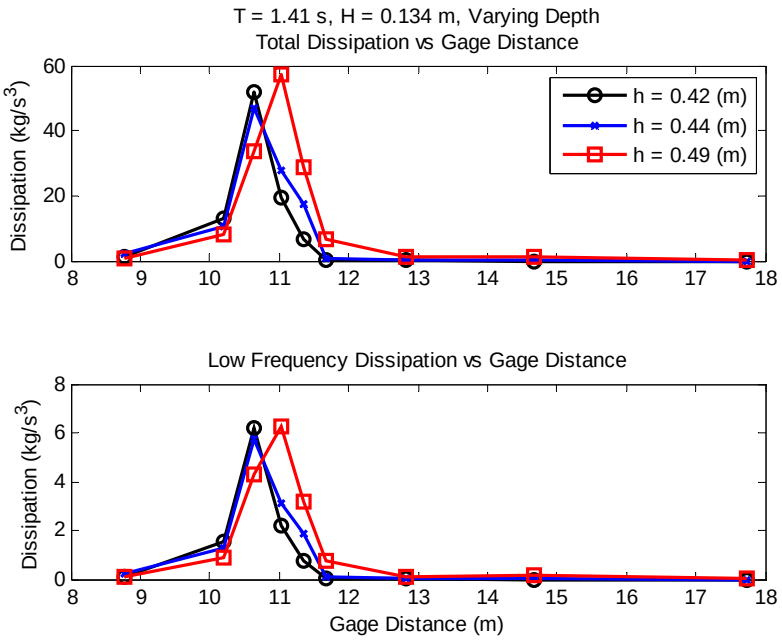

Figure D - 19: Total and Low Frequency Dissipation vs. Gage Locations; Varying Depth; Runs 139, 120, 114

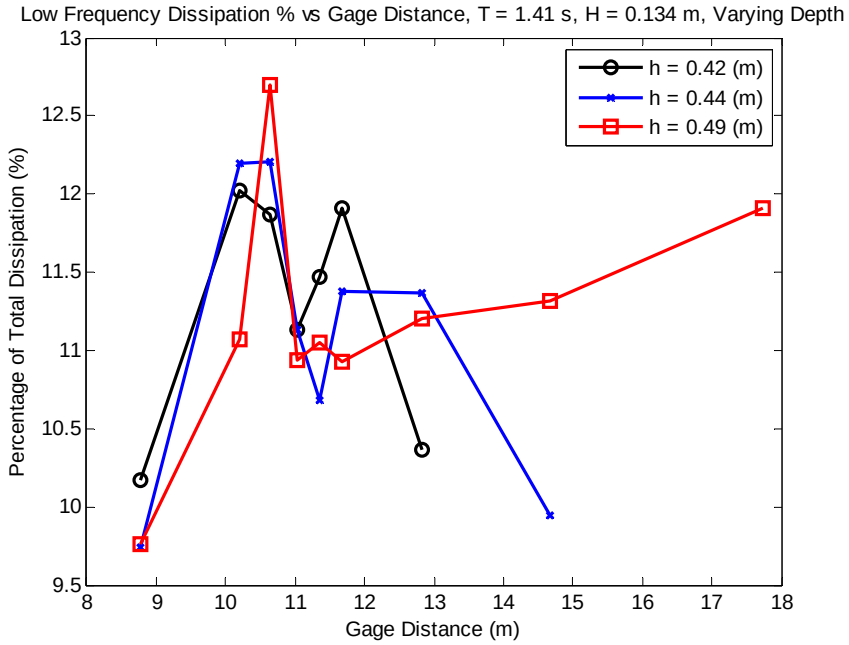

Figure D - 20: Percentage of Total Dissipation Occurring in Low Frequencies; Varying Depth; Runs 139, 120, 114; Also a Spider Waving Goodbye and Thanks for Reading